Design and Evaluation of a Piezoelectric Actuator for Turning

Albert A. Espinoza[1], Luke J. Mayer[2], Paul V. Oberlin[3], Matthew Bement[4]

[1] Dept. of Mechanical Eng., University of Texas at Austin, Austin, TX 78741
[2] Dept. of Mechanical Eng., Texas Tech University, Lubbock, TX 79409
[3] Dept. of Mechanical Eng., Texas A & M University, College Station, TX 77844
[4] Los Alamos National Laboratory, Los Alamos, NM 87545

Nomenclature

E	Young's Modulus
v	Poisson's Ratio
F	Function matrix containing coefficients of cubic equation fit
P	Vector containing material parameters
MO	Vector of the first four experimental frequencies
N	Error metric

ABSTRACT

The machining process of turning is very important for many manufacturing applications. In high precision machining applications, in particular, the surface finish of turned parts is a major concern. Surface finish is strongly correlated with the vibrations and dynamic interactions between the part and the cutting tool. Process characteristics such as spindle speeds, cut depths, feed rates, and part material properties, can vary in real-time and have unexpected and undesirable effects on these vibrations and dynamic interactions. Thus, it is desirable to have a high bandwidth actuator capable of allowing a control system to react to these changing vibration conditions, and result in an improved surface finish. Consequently, this research project focuses on the design and analytical and experimental evaluation of a high bandwidth, high force, low displacement piezoelectric actuator for use between the tool and the tool holder of a conventional computer numerically controlled (CNC) lathe. The dynamic characteristics of the actuator are predicted by creating a finite element model. Next, the baseline performance of the fabricated actuator is characterized experimentally in non-cutting condition environments using tools such as accelerometers and a non-contact laser displacement sensor. Furthermore, the self-sensing capability of the actuator is measured. Finally, the cutting condition performance of the actuator is evaluated in face cutting operations on aluminum rods, and its effects on surface finish are measured using non-contact profilometry. Based on the results from these experiments, the performance characteristics of the actuator are documented for future use in high precision machining operations.

1 INTRODUCTION

1.1 Purpose

Surface finish is an important consideration in any machining process. The quality of the surface influences the performance of the part (e.g. hydrodynamic performance, fatigue life). If unwanted vibrations can be actively controlled, the surface finish can be improved. The goal of this project is to design and test a piezoelectric actuator (fast tool servo) placed between the tool and tool-holder, capable of reacting quickly to conditions at the end of the tool in order to improve surface finish. Because the tool experiences high loads that change quickly, the actuator must be able to operate at high frequencies while applying large forces. Also considering the scale of correction needed, the actuator does not have to provide large displacements. These constraints make a strong case for using a piezoelectric material as the motive source for the fast tool servo.

1.2 Motivation

Typical high-precision turning operations involve a two-step process. The part is first machined in a conventional CNC lathe and then it is further machined in either a grinder or an ultra-precision lathe to meet the desired tolerances. High-precision machining equipment is costly and must be kept isolated from external thermal and vibration effects [4]. Thus, in order to reduce capital costs and machining complexity, the design team would like to be able to use a conventional CNC lathe to achieve a comparable degree of surface quality as a high precision lathe by attaching an actively-controlled tool to the CNC lathe. Furthermore, owing to the fact that conditions between the part surface and the cutting tool change rapidly during the turning operation, the tool design must contain a high-bandwidth actuator that can react quickly to the undesired vibrations that result from these non-uniformities. Piezoelectric actuators have long been used in fast tool servo applications, and the results from these studies have shown that a piezoelectric actuator has the capabilities required to achieve bandwidths of up to 2 kHz with a stroke of 12 μm, while still retaining the required load capacity (in the order of kN) needed for this application [2].

1.3.1 Background

The machining industry requires precision cutting that comes in many forms. Each process is limited by unwanted vibrations, which occur as a result of high speeds, feed rates, cut depths, and part material properties. These vibrations are often referred to as chatter. Chatter is an unwanted side effect of cutting that decreases surface finish quality and reduces tool life. A solution to this problem involves using a piezoelectric actuator to damp the vibrations. Several research studies have used this type of fast tool servo to improve their respective cutting process.

Boring has been historically limited by bar vibrations that occur when the length-to-diameter ratios of the boring bar are large. As the boring bar length increases, the vibrations that occur at the cutting end are amplified, and therefore the depth and diameter that can be bored is limited. By using piezoelectric actuators, Browning et al. [1] were able to increase bar length-to-diameter ratios, feed rates, depth of cuts and cutting speeds beyond that which passively-damped systems are capable of achieving. Two accelerometers were placed near the cutting tip of the boring bar and used to collect the data needed to actively damp the bar at its top. This damping was accomplished by attaching four piezoelectric actuators placed in opposition to each other within the bar clamp, one set to provide tangential damping and the other set to provide a normal damping component. The success of this process is seen in its results: the maximum boring depth of a high-temperature nickel alloy increased by 400% while maintaining desired surface finish.

Using a piezoelectric actuator, Zhu et al. [2] developed a process of precision shaft cutting using a conventional CNC lathe. By using this actuator to better control the movement of the lathe, the process successfully combines the processes of first draft cutting and precision cutting, which saves both time and the expense that is needed to accommodate two separate processes. The piezoelectric actuator acted as a pivoting device for the tool holder, which provided a greater displacement (but less force) for the cutting tool because of the moment arm created.

Flexures allow the tool holder its pivoting movement. A laser and a mirror system were utilized on the back of the tool holder to follow and control the precise movement of the tool head. Using this process, Zhu et al. successfully produced shafts with surface finishes equivalent (R_{max} < 2.5 µm, where R_{max} is the peak to valley distance) to that of grinding machines or precision lathes.

A design similar to the one being proposed in this study was implemented by Kim and Kim [3] in their research concerning feed-forward control of fast tool servo for real-time correction of spindle error in diamond turning of flat surfaces. By using a piezoelectric actuator in a lathe head and placing a capacitive displacement sensor directly beneath the tool holder, a diamond tipped tool was used to fabricate flat aluminum pieces of up to 100 mm in diameter with a peak-to-valley accuracy of 0.10 µm.

In this current design, the fast tool servo will first be simulated using a finite element model to give insight into operating frequency ranges. The actuator will then be tested in a lab environment to establish its performance and validate the FE model. Finally the actuator will be attached to a CNC lathe and tested. While attached to the lathe, facing operations will be done with the actuator powered off, the actuator powered at a constant frequency and then with the actuator put through a voltage sine sweep.

2. EXPERIMENT

2.1 Apparatus

The apparatus used in the experimental setup consists of the lathe tool assembly. The lathe tool is comprised of the cutting tool piece, tool holder assembly, diaphragm, piezoelectric stack, preload piece and supporting shell structures. Three diaphragms of nominal thicknesses of 1.5875 mm, 3.1750 mm and 4.7625 mm (1/16”, 1/8”, and 3/16”) were tested on the assembly. All of these components can be seen in Figure 1.

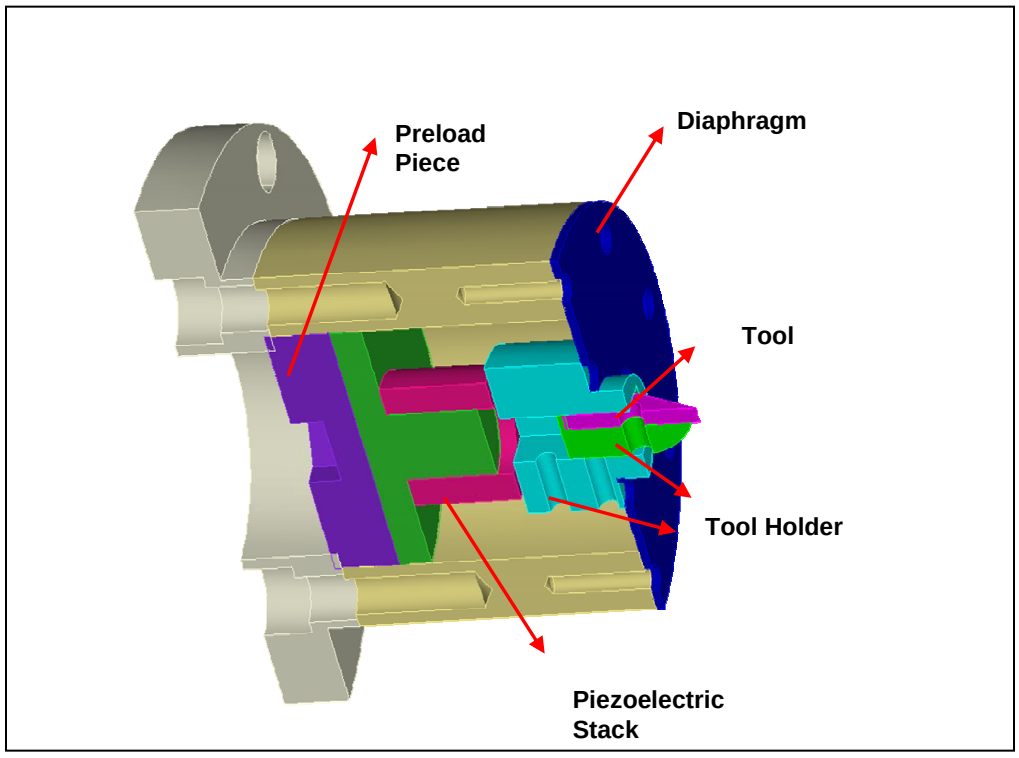

Figure 1. Labeled Cross-Section of Lathe Tool Assembly

Several instruments were used to test the lathe tool assembly and determine its dynamic characteristics. A Photon DACTRON was used for all the data acquisition involved with the modal tests. A Keyence LC -2400A laser displacement system measured piezoelectric hysteresis and a FLIR Thermacam was used for observing the piezoelectric thermal characteristics. A model 354C10 ICP tri-axial accelerometer was used to measure the response of the assembly. The piezoelectric stack used in the design was the HPSt 500/10-5/15 model. Piezoelectric stack specifications can be seen in Appendix B. For the cutting testing, a NI 6052E PCI data acquisition card, used in conjunction with the Matlab Data Acquisition Toolbox, was employed for the data collection.

2.2 Procedure

2.2.1 Modal Tests

Three different diaphragms of 1.5875 mm, 3.1750 mm and 4.7625 mm (1/16", 1/8", and 3/16") nominal thicknesses were tested individually for each setup. The first component of the modal tests was to perform a free-free impact test of each diaphragm. Each diaphragm was suspended by 25 cm lengths of 6.8 Kg (15 lb) fishing string and impacted with a PCB 086D80 model miniature instrumental impulse hammer at four equidistant points from the center of the diaphragm. A single axial accelerometer was wax mounted to the diaphragms at a point closest to the center. The tool assembly was then mounted to the diaphragms and the procedure was repeated with an additional impact at the back of the tool assembly. In this test and the following tests a tri-axial accelerometer was fixed to the rectangular mock cutting piece instead of a single-axis, wax-mounted accelerometer. This setup is shown in figure 2. For the final modal test, the fully assembled FTS was placed on foam as shown in Figure 3 and impacted in the same four previously described locations.

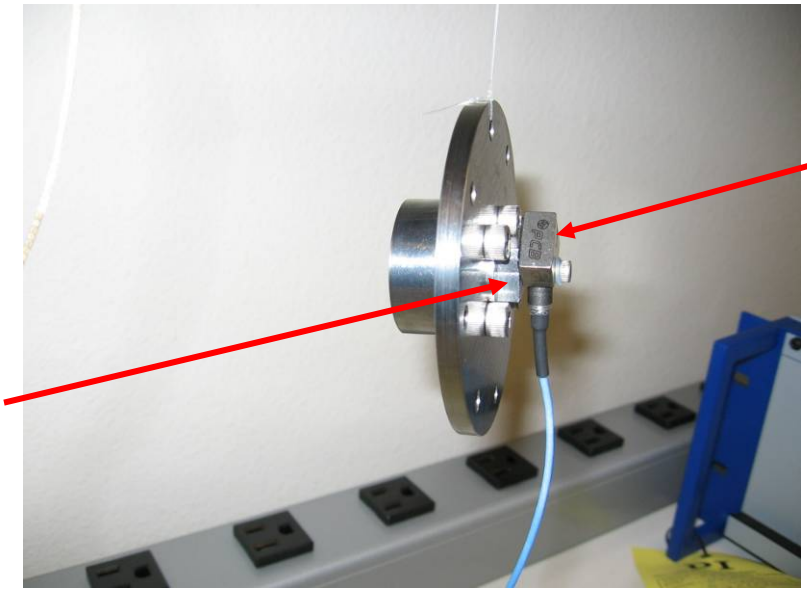

Figure 2. Diaphragm Assembly in Free-Free condition

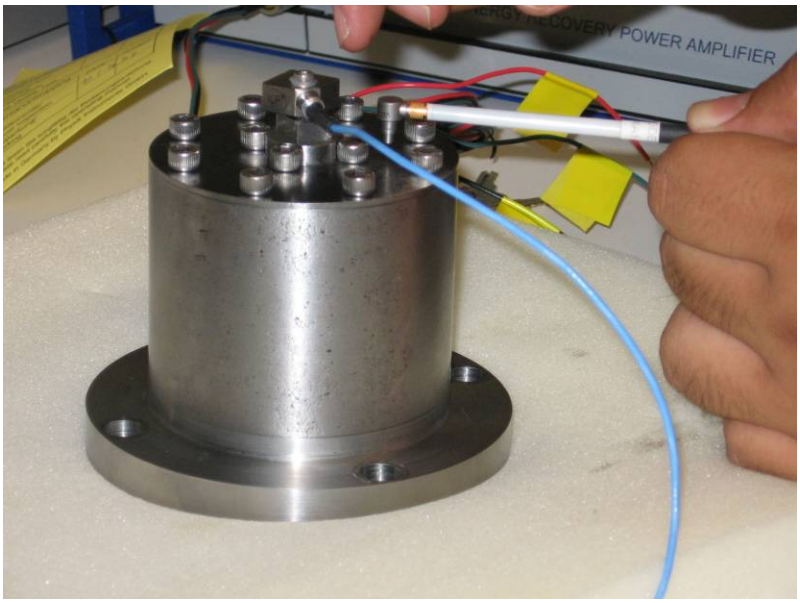

Figure 3. Assembled Fast Tool Servo on foam

By performing the free-free test first, the accuracy of the model could be validated with no external damping sources and no non-linear boundary conditions. Once the free-free analytical model was properly modified to closely capture the dynamics of the experimental data, the dynamics of the metal casing and the bolted boundary condition could be introduced to the FE model of the diaphragm assembly and compared to the corresponding experimental data. Any inconsistencies in this second comparison were then attributed to an inaccurate modeling of the boundary conditions.

After all the components were tested without the piezoelectric stack, the complete, assembled FTS was tested. The FST was fully assembled and the piezoelectric stack was placed inside. The actuator has four wire leads. The red (+) and black (-) leads are the voltage input wires, and these wires were connected to the output terminals from a 200 V, 50mA amplifier. The light blue terminals are the PZT sensor output connections. These wires were directly connected to one of the input channels of the DACTRON data acquisition board. This signal was used to determine the FTS frequency response. Furthermore, a tri-axial accelerometer was attached at the location of the tool tip to provide a second frequency response input signal to the DACTRON board. The full setup is shown in Figure 4.

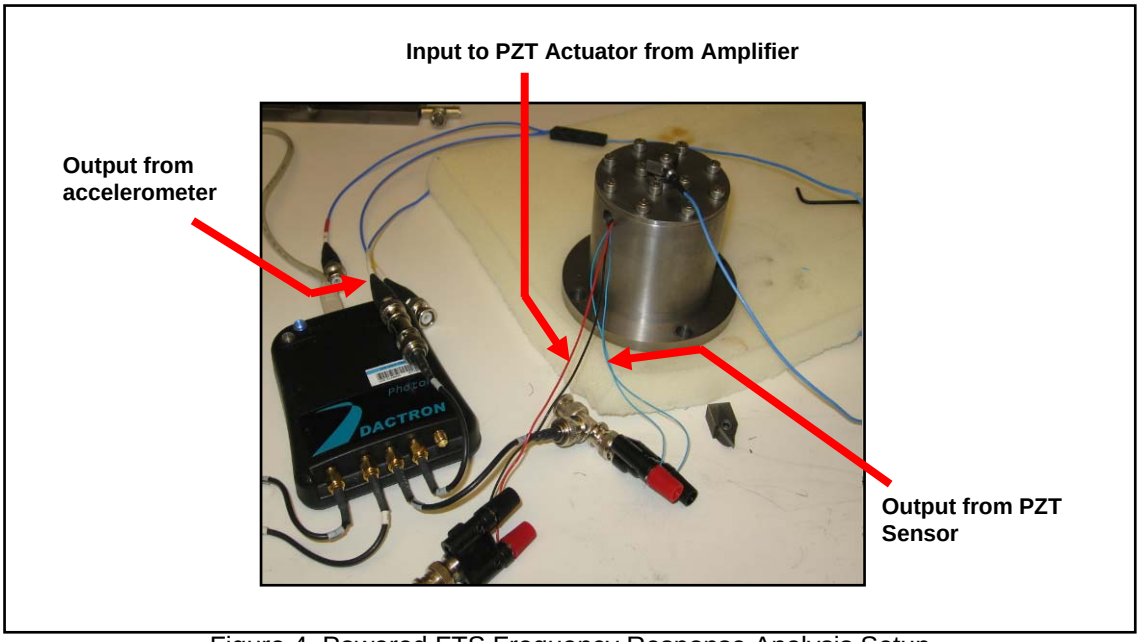

Figure 4. Powered FTS Frequency Response Analysis Setup

A burst random signal excitation was applied to the PZT stack and the final response collected was an average of 100 individual responses. The same experiment was performed for each of the different diaphragm thicknesses.

2.2.2 Piezoelectric Hysteresis

Piezoelectric hysteresis was tested by applying a voltage in increasing and decreasing increments to the fully assembled FTS via a 1000 volt DC amplifier. A Keyence LC-2400A laser displacement sensor measured the displacement of the tool tip. The voltage was augmented in increments of 100V until reaching 1000 V and then reversed back toward 0 V. This cyclical voltage process was repeated three times for each diaphragm to test for repeatability.

2.2.3 Thermal Piezoelectric Characteristics

The thermal characteristics of the piezoelectric stack were tested with the FLIR SC500 Thermacam and a 1000 volt amplifier. The piezoelectric stack was fixed under a C-clamp against the table to simulate the fixed condition the piezoelectric is in when fully assembled in the lathe assembly. Using the amplifier, 500 volts was applied to the piezo stack at a frequency of 1000 Hz while the Thermacam took continuous pictures. The voltage was applied until the piezoelectric stack reached a temperature of 49 C (120 F). The lab setup of this process is shown in Figure 5 below.

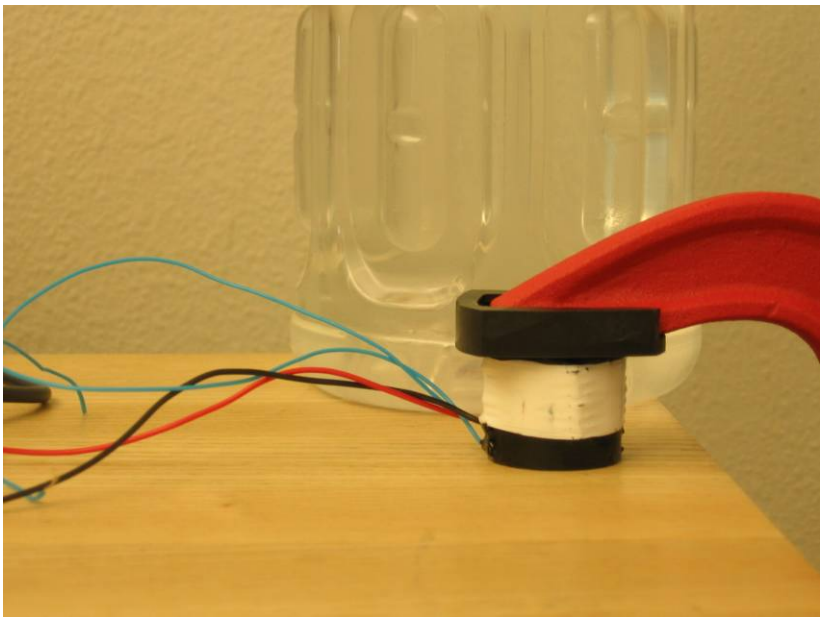

Figure 5. Piezoelectric Thermal testing Set up

It can be noted that a water bottle filled with cold water was placed behind the piezoelectric stack to provide thermal contrast with the stack's surroundings, and enable the camera to focus on the stack before any heat was generated by it.

2.2.4 Facing Cuts with Fast Tool Servo

The final testing comprised of performing facing cuts on aluminum rods. Three different cuts were executed and compared for surface finish. The first facing cut was performed to simulate a cut from an un-modified conventional CNC lathe. The second cut utilized the lathe with the FTS attached, however, with no voltage applied to the piezoelectric stack during the cut. Next a cut was made with a constant 2 kHz signal applied to the FTS. Finally, a cut was made with the system attached to the lathe while a sine swept voltage was applied to the FTS. The surface of each of these cuts was then analyzed using white light profilometry.

3. RESULTS

3.1 Modal Tests

The responses of the principal moving components of the actuator were characterized by performing free-free impact tests to verify the unconstrained FE model. The data sets were processed in ME Scope and the resonant peaks, damping values, resonant magnitudes and resonant phases for each mode were attained for the three diaphragms as shown in Tables 1-3. The comparison between this experimental data and the finite element model results will be discussed in subsequent sections.

Tables 1-3 demonstrate that as the diaphragm thickness increases, the FTS natural frequencies also increase. For instance, for the fully assembled FTS tests, the frequency of the first mode more than doubles from 2.24e3 to 2.88e3 Hz as the thickness doubles from 1.5875 to 3.1750 mm. Another important aspect to note, however, is that as the thickness increased from 3.1750 mm to 4.7625 mm, the change in the first natural frequency only increased slightly from 4.88e3 to 5.00e3 Hz. Thus, further increase in thickness is not a significant way of increasing the frequency of the first mode after a certain point.

Table 1. Modal Experiment Data for 4.7625 mm Diaphragm

4.7625 mm (3/16") Diaphragm				
Fixed Diaphragm Assembly - Unmounted				
Mode	Frequency (Hz)	Damping	Res. Mag.	Res. Phase
1	5.00E+03	0.0268	809	172
2	6.56E+03	0.68	3.67E+04	270
3	8.29E+03	0.196	1.22E+04	226
4	9.92E+03	0.954	1.78E+04	281
Free Diaphragm Assembly				
Mode	Frequency (Hz)	Damping		Res. Mag.
1	4.70E+03	0.0288	5.20	10.9
2	5.50E+03	0.303	2.94E+02	249
3	5.63E+03	0.224	8.68E+02	250
4	6.12E+03	0.503	1.31E+03	63.8
Diaphragm				
Mode	Frequency (Hz)	Damping	Res. Mag.	Res. Phase
1	3.83E+03	0.0131	661	321
2	6.21E+03	0.0163	1.11E+02	207
3	7.65E+03	0.00163	1.05E+00	23.8
4	9.31E+03	0.0169	5.26E+01	56.9

Table 2. Modal Experiment Data for 3.1750 mm Diaphragm

3.1750 mm (1/8") Diaphragm				
Fixed Diaphragm Assembly - Unmounted				
Mode	Frequency (Hz)	Damping	Res. Mag.	Res. Phase
1	4.88E+03	0.0332	62.4	227
2	5.57E+03	0.0396	77.7	38.1
3	6.04E+03	0.494	1.97E+04	241
4	7.25E+03	0.996	4.11E+04	108
Free Diaphragm Assembly				
Mode	Frequency (Hz)	Damping	Res. Mag.	Res. Phase
1	4.12E+03	0.338	4.48E+04	328
2	4.22E+03	0.194	5.11E+04	330
3	4.44E+03	0.732	2.63E+04	286
4	5.53E+03	0.451	1.70E+05	339
Diaphragm				
Mode	Frequency (Hz)	Damping	Res. Mag.	Res. Phase

1	2.46E+03	0.0143	71.6	37.9
2	3.91E+03	0.0403	3.90E+06	170
3	5.93E+03	0.0468	3.39E+01	287
4	8.55E+03	0.122	1.48E+03	223

Table 3. Modal Experiment Data for 1.5875 mm Diaphragm

1.5875 mm (1/16") Diaphragm				
Fixed Diaphragm Assembly - Unmounted				
Mode	Frequency (Hz)	Damping	Res. Mag.	Res. Phase
1	2.24E+03	1.17	1.47E+04	207
2	2.89E+03	1.21E+00	3.50E+04	191
3	5.66E+03	1.74E+00	1.29E+04	40.3
4	7.09E+03	7.88E-01	3.24E+04	100
Free Diaphragm Assembly				
Mode	Frequency (Hz)	Damping	Res. Mag.	Res. Phase
1	2.19E+03	0.350	4.71E+04	335
2	2.50E+03	0.129	1.36E+04	342
3	2.73E+03	1.04	9.90E+04	352
4	2.98E+03	0.426	6.57E+04	3.51
Diaphragm				
Mode	Frequency (Hz)	Damping	Res. Mag.	Res. Phase
1	1.28E+03	0.0276	249	185
2	2.04E+03	0.0466	7.25E+01	193
3	3.17E+03	0.00785	3.33E+02	96.6
4	4.58E+03	0.0957	1.77E+03	14.0

3.1.1 Finite Element Model Verification

In an effort to better model the behavior of the fast tool servo, several sets of experimental results were compared to similar results obtained with an analytical model. Three modal tests were performed: free-free diaphragm, free-free diaphragm assembly and assembled FTS on foam. Modal tests were performed in order of increasing number of constraints in order to separate boundary conditions from the dynamics of the system. This arrangement was done so that the model results could first be correlated to results obtained from the simplest configuration. Next, this correlation study was extended to the results of more complex dynamic interactions that could then be characterized in a step by step manner. The first step to validating the model was to measure as many physical parameters of the system as possible. Each part was weighed and each diaphragm thickness was measured with a micrometer. The data were then input into the free-free diaphragm model along with generic

material properties obtained from literature. The two unknown material properties were the elastic modulus (E) and Poisson's ratio (*v*) of the diaphragm. To determine the sensitivity of the model to these two parameters, eight simulations were run: four were varying E and holding *v* constant and four holding *v* constant while varying E. A cubic equation was then fit to map the inputs to the first four modal frequencies of the model. In order to determine the optimal values for the two parameters, a range of values in the vicinity of the generic values were evaluated according to the following equation:

$$N=||(F*P-M0)./M0||^2 \quad (1)$$

Where F is the function matrix containing the coefficients of each term in the cubic equation fit to the first four modal frequencies of the model, P is the vector containing the two material parameters (the terms of the cubic fit equation), M0 is the vector of the first four experimental modal frequencies and N is an error metric. The two material parameters of E and *v* that minimize N in the range of interest are the most optimal for the model.

First, the frequencies were extracted from the modal test data using a peak fitting method. The results can be seen above in Tables 1-3. These values will form the M0 vector from equation 1. After the equations were fit, "N" from equation 1 was plotted versus the two unknown parameters. The plot for the free-free, 4.7625 mm thick diaphragm is shown in Figure 5.

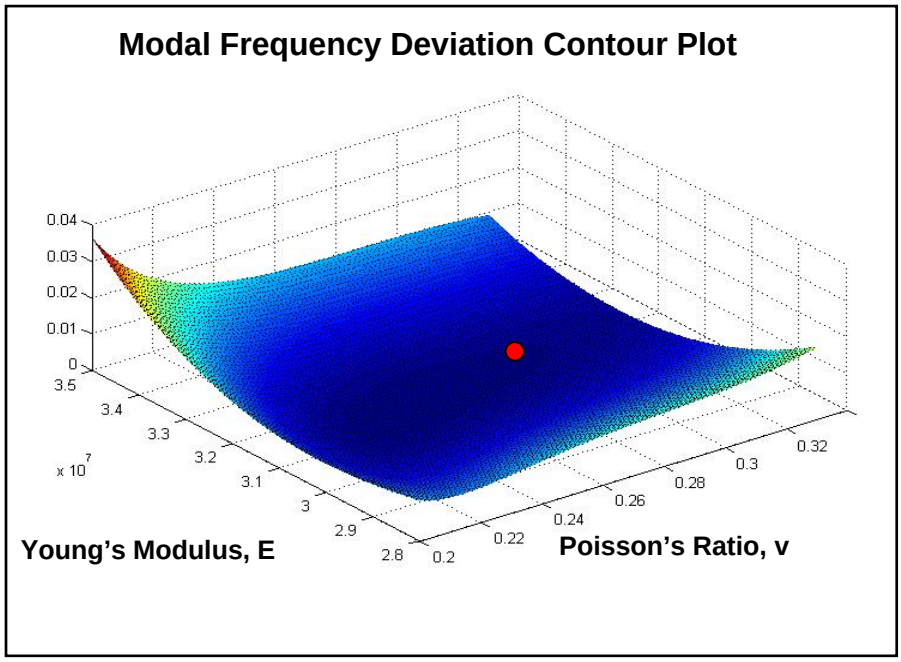

Figure 5. Modal Frequency Error Variation

The red dot in Figure 5 denotes the minimum error metric "N" which corresponds to the optimal values for E and *v*: 222 GPa (3.22e7 psi) for the former and 0.28 for the latter. These values were then input into the free-free diaphragm model in ABAQUS. The results of these simulations can be seen below in Tables 4-6.

Table 4. Modal Frequencies for 4.7625 mm Diaphragm

4.7625 mm (3/16") Diaphragm	
Mode	**Frequency (Hz)**
1	3.80E+03
2	3.83E+03
3	6.26E+03
4	9.26E+03

Table 5. Modal Frequencies for 3.1750 mm Diaphragm

3.1750 mm (2/16") Diaphragm	
Mode	Frequency (Hz)
1	2.44E+03
2	2.46E+03
3	4.00E+03
4	6.02E+03

Table 6. Modal Frequencies for 1.5875 mm Diaphragm

1.5875 mm (1/16") Diaphragm	
Mode	Frequency (Hz)
1	1.27E+03
2	1.28E+03
3	2.08E+03
4	3.15E+03

It can be seen from Tables 1-3 and Tables 4-6 that the analytical modal frequencies are all within 10% of the experimental modal frequencies, except for one. The exception is the third experimental mode in the 4.7625 mm diaphragm, which does not show up in the FE model. Furthermore, the FE simulation predicts the first two modes to be very close together. This can explain why the third and fourth modes obtained from the model correspond to the second and third modes, respectively, obtained from the modal experiments. Because only one accelerometer was used for the modal tests, it is reasonable to suspect that the test data did not show the two close peaks, but just one peak composed of the superposition of the first two modes. It is also known that the two close modes are the result of the symmetry. For the following two configurations (free-free diaphragm and tool assembly, and fully constrained FTS) the only model parameter that could be optimized was the equivalent constrained surface. For the free-free diaphragm and tool assembly, the constrained surface that was modified was the front face of the tool holder assembly and its mating surface on the diaphragm. This surface can be seen below in Figure 6. The effect of varying the outer radius of the constrained surface was evaluated by running models at five different radii for each diaphragm. This data were then mapped to the first three experimental modal frequencies in a procedure identical to that done for the free-free diaphragm above. The optimal radius was then calculated. The results can be seen in Tables 7-9.

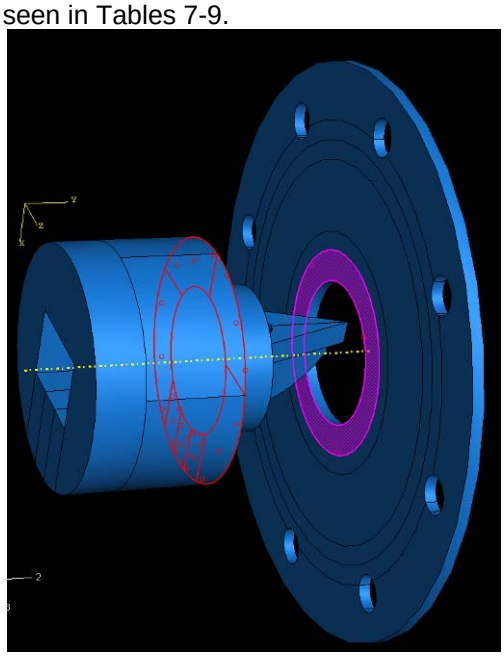

Figure 6. Constrained surface for free-free Diaphragm and Tool Assembly

Table 7. Free-free thin diaphragm and tool model results

1.5875 mm (1/16") Diaphragm and Tool	
Mode	**Frequency (Hz)**
1	**2167**
2	**2269**
3	**2735**

Table 8. Free-free medium diaphragm and tool model results

3.1750 mm (1/8") Diaphragm and Tool	
Mode	**Frequency (Hz)**
1	**4118**
2	**4124**
3	**4249**

Table 9. Free-free thick diaphragm and tool model results

4.7625 mm (3/16") Diaphragm and Tool	
Mode	**Frequency (Hz)**
1	**5099**
2	**5111**
3	**5705**

For the fully constrained FTS model, the constrained surface modified was the outer ring of the diaphragm that was bolted to the housing. This surface can be seen below in Figure 7. The effect of varying the inner radius of the constrained surface was evaluated by running models at four different radii for each diaphragm. This data was then, again, mapped to the first two experimental modal frequencies using the same procedure as the previous two configurations. These results can be seen below in Tables 10-12.

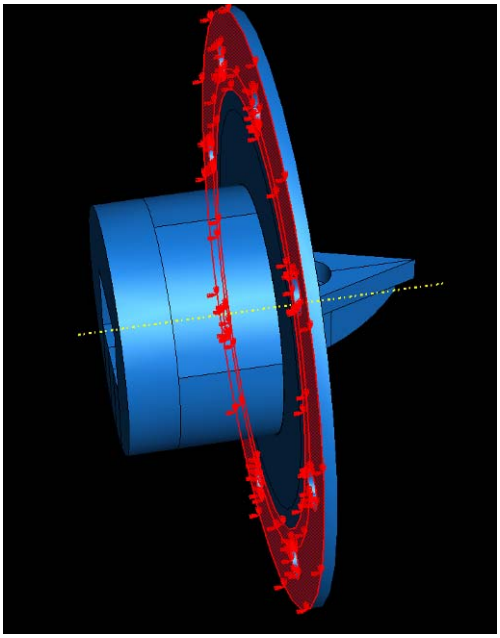

Figure 7. Constrained surface for constrained diaphragm assembly

Table 10. Constrained thin diaphragm and tool model results

1/16" (1.5875 mm) Assembly	
Mode	**Frequency (Hz)**
1	**2241**
2	**2634**

Table 11. Constrained medium diaphragm and tool model results

1/8" (3.175 mm) Assembly	
Mode	**Frequency (Hz)**
1	**5002**
2	**5822**

Table 12. Constrined thick diaphragm and tool model results

3/16" (4.7625 mm) Assembly	
Mode	**Frequency (Hz)**
1	**4997**
2	**5179**

3.2 Piezoelectric Hysteresis

The resulting displacement from an applied DC voltage to the assembled FTS was measured with a LC-2400A Keyence laser displacement sensor and recorded for each diaphragm. The displacement in micrometers was plotted against the applied voltage for each diaphragm. The LC-2400A Keyence laser displacement sensor has a resolution of half of a micron, and was seen to have a random value variance of approximately 1.5 microns. As can be seen from the sample Figure 6 below, the maximum hysteresis values from each cycle are approximately 2 µm. It is therefore conclusive that the analysis of the hysteresis exceeds the accuracy of this displacement sensor and a more sensitive sensor would be required to further study the hysteresis effect.

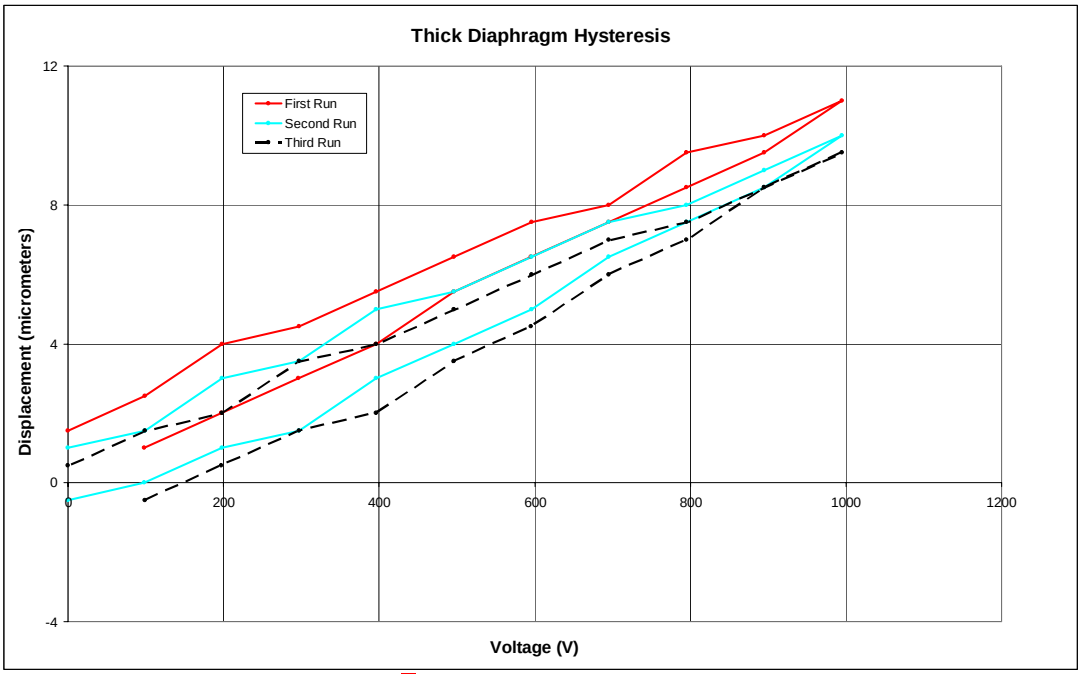

Figure 8. Thick Diaphragm Hysteresis

The piezoelectric hysteresis testing was not without its use. The displacement measurements provided diaphragm displacement values at 1000V that had consistency to within 2 microns. The thin diaphragm was seen to have a resulting displacement of 17-18.5 µm, the middle diaphragm 12.5-13.5 µm, and the thick diaphragm 9-9.5 µm. These values provide a value of maximum displacement that can be expected from each of the diaphragms. Additional hysteresis plots can be seen in Appendix A.

3.3 Thermal Piezoelectric Characteristics

As a result of time constraints (caused by the dysfunctional amplifier) the only thermal testing that was done was of the piezoelectric stack by itself. Originally, thermal testing was also to be done on the fully assembled lathe tool to see how much heat was transferred from the piezo stack to the tool tip. This data would have then been matched with FE thermal model temperature spectrum of the diaphragm and tool assembly to see how well it predicted temperature spectrums.

A 1000 volt amplifier was used to provide 500 volts to the piezoelectric stack at 4000 Hz. The voltage was applied until the piezoelectric stack reached 49 C (120 F), which took approximately 22 seconds. A continuous set of frames were captured during the test and three sample frames are shown below in Figure 7.

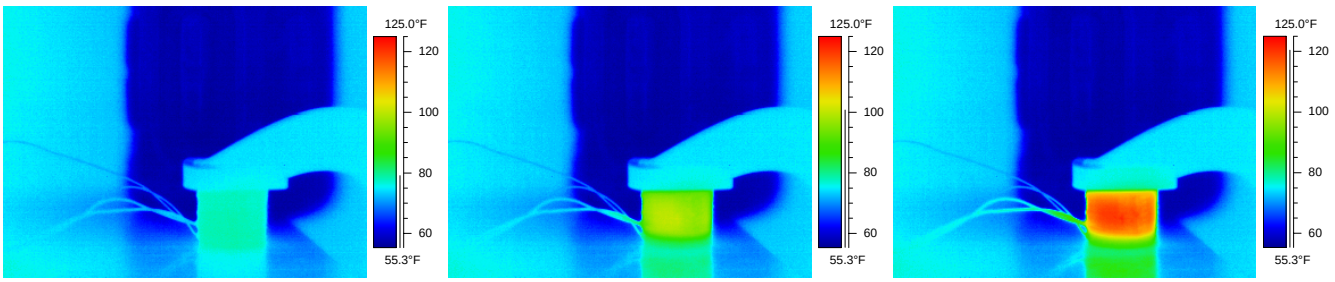

Figure 7. Infrared pictures of activated piezoelectric stack

The thermal data that is of interest in respect to this project is the rate at which the piezoelectric stack increases its temperature with time. Sample frames were selected from the images captured by the FLIR camera and their respective time and temperature values were retrieved and plotted in Figure 8.

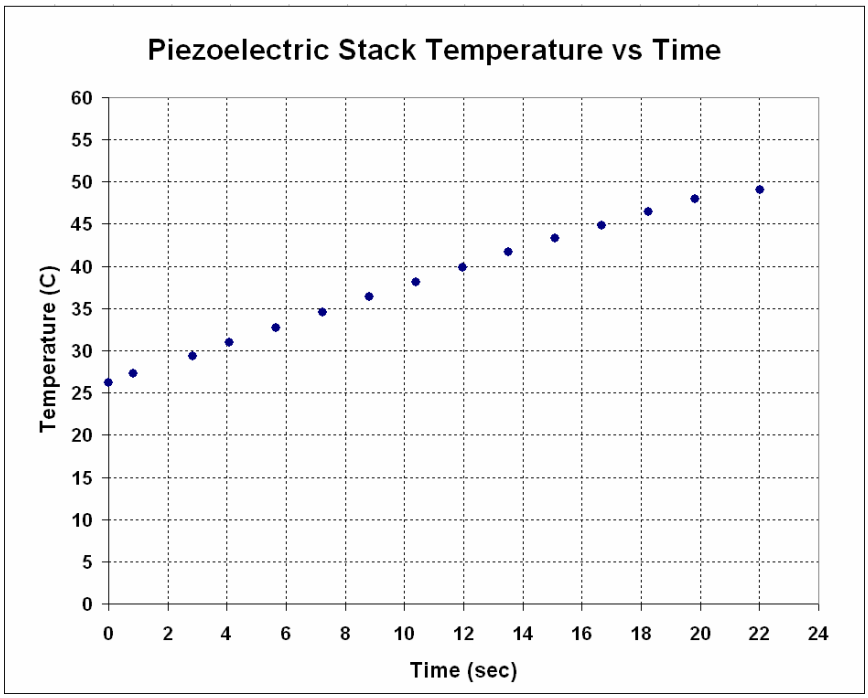

Figure 8. Piezoelectric Stack Temperature in Time

It is seen in Figure 8 that the temperature varies linearly with time within the temperature spectrum tested. This is a positive result because the temperature spectrum should begin an exponential climb .

3.4 Cutting Tests

Al 6061 was selected for the cutting tests because of its better machinability. The unpowered facing cut using the thick diaphragm was then repeated. A spectrogram of the voltage output from these tests can be seen in Appendix C. In the second series of tests, the thick diaphragm was replaced with the thin diaphragm (1.5875 mm, 1/16" nominal). First, an unpowered facing cut was performed. Then three sets of data were taken from the same aluminum sample at a decreasing radius from the axis of rotation with the FTS powered with a constant 2kHz sine wave. The last test consisted of three sets of data taken at a decreasing radius from the axis of rotation with a sine sweep from 100Hz to 10kHz applied to the FTS . Spectrograms of all cutting tests can be seen in Appendix C. In the spectrograms from the sine-swept tests the frequencies of the resonances seem to "bounce" off of 10kHz. This is because the voltage measured from the piezo-sensor was unfiltered and the sampling rate of 20kHz causes aliasing of any frequency above 10kHz.

3.4.1 Profilometry

Each sample that was faced was measured in a white light profilometer to evaluate surface roughness. This data was then opened in MATLAB and because the profilometer is unable to measure some points bad data points were replaced by interpolation of adjacent data points. The feature of interest contained in these samples was the shape of the cut depth in order to observe any effect caused by powering the FTS. In order to help detect the presence of any specific spatial frequencies a fast fourier transform (FFT) was applied to 600 separate vertical strips of surface data since the tool paths was oriented in a roughly vertical direction and all of these FFT graphs were averaged to produce a final FFT. Surface profiles, vertical strip profiles and surface FFT graphs can be seen in Appendix D.

4. Discussions

A notable feature seen in the spectrograms is the attenuation of even numbered resonances of the forcing function. The thin plate also appears to have two resonances and one anti-resonance near 5kHz. It also seems that the lathe had resonances around 6kHz and 8.5 kHz as there is power around these frequencies in every test regardless of the diaphragm used. Another interesting feature is that in the tests taken at the outer edge of the Al 6061 sample two response frequencies appear that start at one frequency and settle to a different frequency and then die out as they are not prevalent in data taken closer to the axis of rotation. For the thick plate these signals start at 6 and 7 kHz and for the thin plate they appear at 4.5 and 7.5 kHz.
The surface profilometry data appears to be inconclusive. No set of data stands out as unique. In terms of surface roughness each sample appears to have roughly equivalent surface quality.

5. Conclusions

Although the results appear to be inconclusive, it should be noted that an effect on surface finish in the sample faced with the FTS running at 2kHz could be seen with the naked eye as a band near the center and to a lesser extent at a larger radius, which can be seen below in Figure 9.

Figure 9. Sample faced with FTS running at 2khz

Since a change in surface finish could not be detected analytically it may be worth using a higher power system. These tests had originally been designed to use an amplifier capable of producing 1000V at 200mA, however due to this particular amplifier's untimely malfunction, a much less powerful amplifier that produced a maximum of 200V at 50 mA (20 times less power) was used in the cutting tests. It should also be noted that the average surface roughness of each test is very similar as seen below in Table 13, suggesting that at the very least the addition of the FTS to the lathe was not detrimental to surface finish.

Table 13. Surface roughness of all test samples

Surface roughness of test samples (microns)	
Thick Diaphragm, Unpowered	**6.3, 6.1**
Thin Diaphragm, Unpowered	**5.2, 5.1**

Thin Diaphragm, 2kHz	**5.4, 5.3**
Thin Diaphragm, Sine Sweep	**6.0, 6.4**

6. ACKNOWLEDGEMENTS

Special thanks to Dr. Pete Avitable for guidance on the modal testing and frequency response, Dr. Don Leo for guidance and suggestion of the naked piezoelectric tests and Dr. Matt Bement for his mentorship. We would also like to recognize the help of Dr. Gyuhae Park in setting up the high voltage amplifier and for his advice on piezoelectric actuation.

REFERENCES

[1] Browning D R, Golioto I and Thompson N B 1997 Active chatter control system for long-overhang boring bars *Smart Structures and Materials 1997; Industrial and Commercial Applications of Smart Structures Technologies* vol 3044 ed J M Sater (Bellingham, WA: SPIE Optical Engineering Press) pp 270-80.

[2] Zhu W-H, Jun MB, Altintas Y. A fast tool servo design for precision turning of shafts on conventional CNC lathes. Int J Machine Tools Manufact 2001;41:953-65.

[3] Kim H-S, Kim E-J. Feed-forward control of fast tool servo for real-time correction of spindle error in diamond turning of flat surfaces. Int J of Mach Tools Manuf 2003;43(12):1177-83.

[4] Woronko A, Huang J, Altintas Y. Piezoelectric tool actuator for precision machining on conventional CNC turning centers. Prec Eng 2003;27:335-45.

APPENDIX A: Piezoelectric Stack Hysteresis Charts

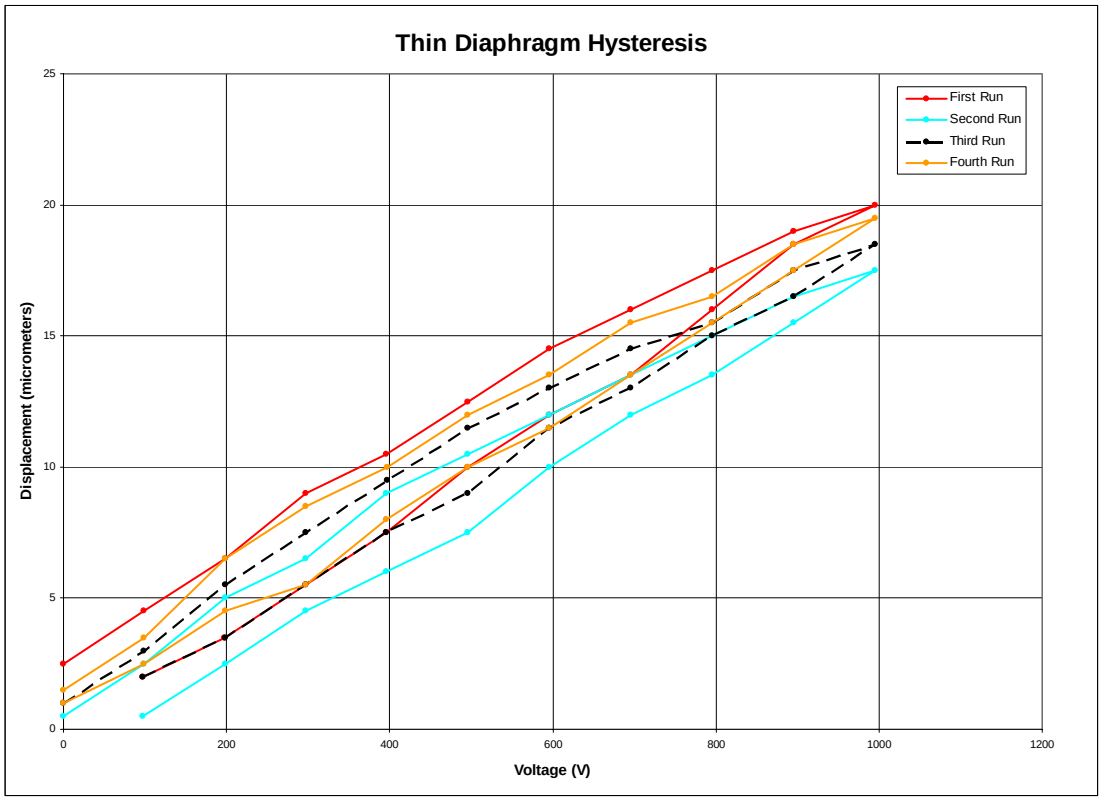

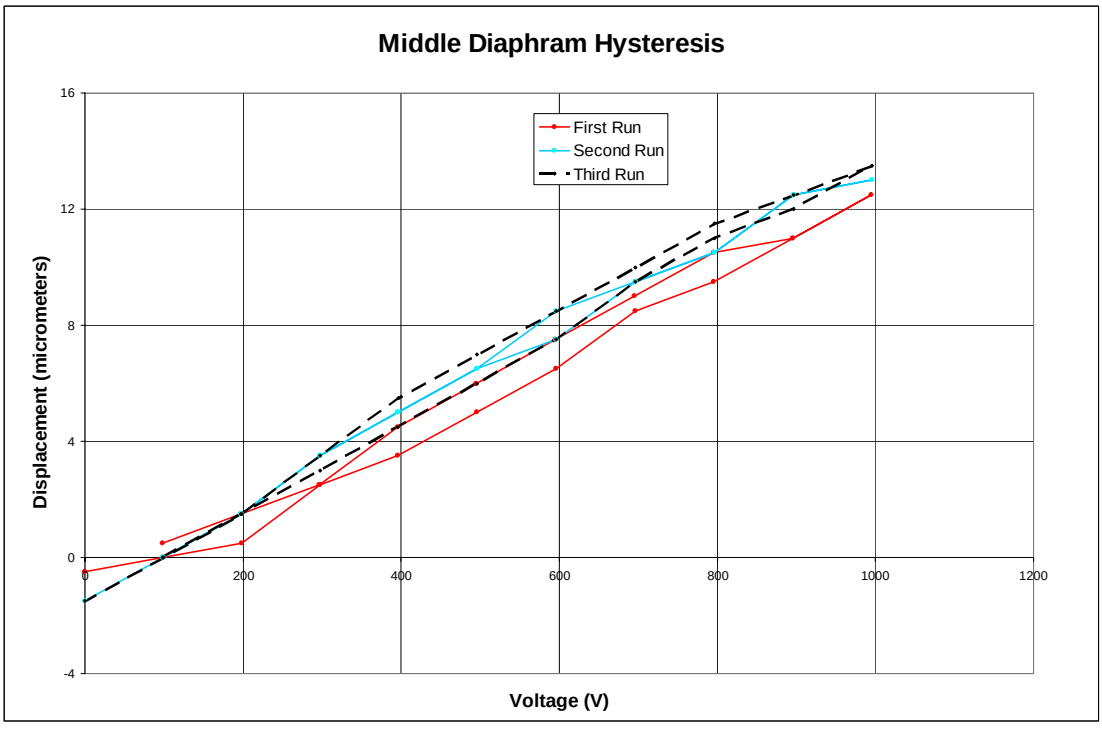

APPENDIX B: Piezoelectric Stack Specifications

HPSt 500/10-5/... und HPSt 1000/10-5/...

Maximum load: 3500 N
Maximum force generation: 2800 N
Open loop sensitivity for 5 mV noise for actuator HPSt 500/10-5/5: approx. 0.05 Nanometer

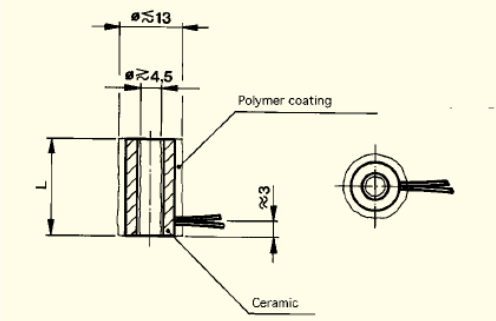

Type	max. stroke µm	length L mm	el. capacitance nF	stiffness N/µm	resonance frequency kHz
HPSt 500/10-5/5	12/7	9	65	200	40
HPSt 500/10-5/15	25/17	18	180	100	25
HPSt 500/10-5/25	35/25	27	260	70	20
HPSt 500/10-5/40	55/40	36	350	50	15
HPSt 500/10-5/> 40	> 40	on request			
HPSt 1000/10-5/5	13/8	9	15	210	50
HPSt 1000/10-5/15	25/17	18	40	110	35
HPSt 1000/10-5/25	35/25	27	65	75	25
HPSt 1000/10-5/40	55/40	36	90	55	20
HPSt 1000/10-5/60	80/60	54	140	35	15
HPSt 1000/10-5/>60	> 60	on request			

APPENDIX C: Cutting Test

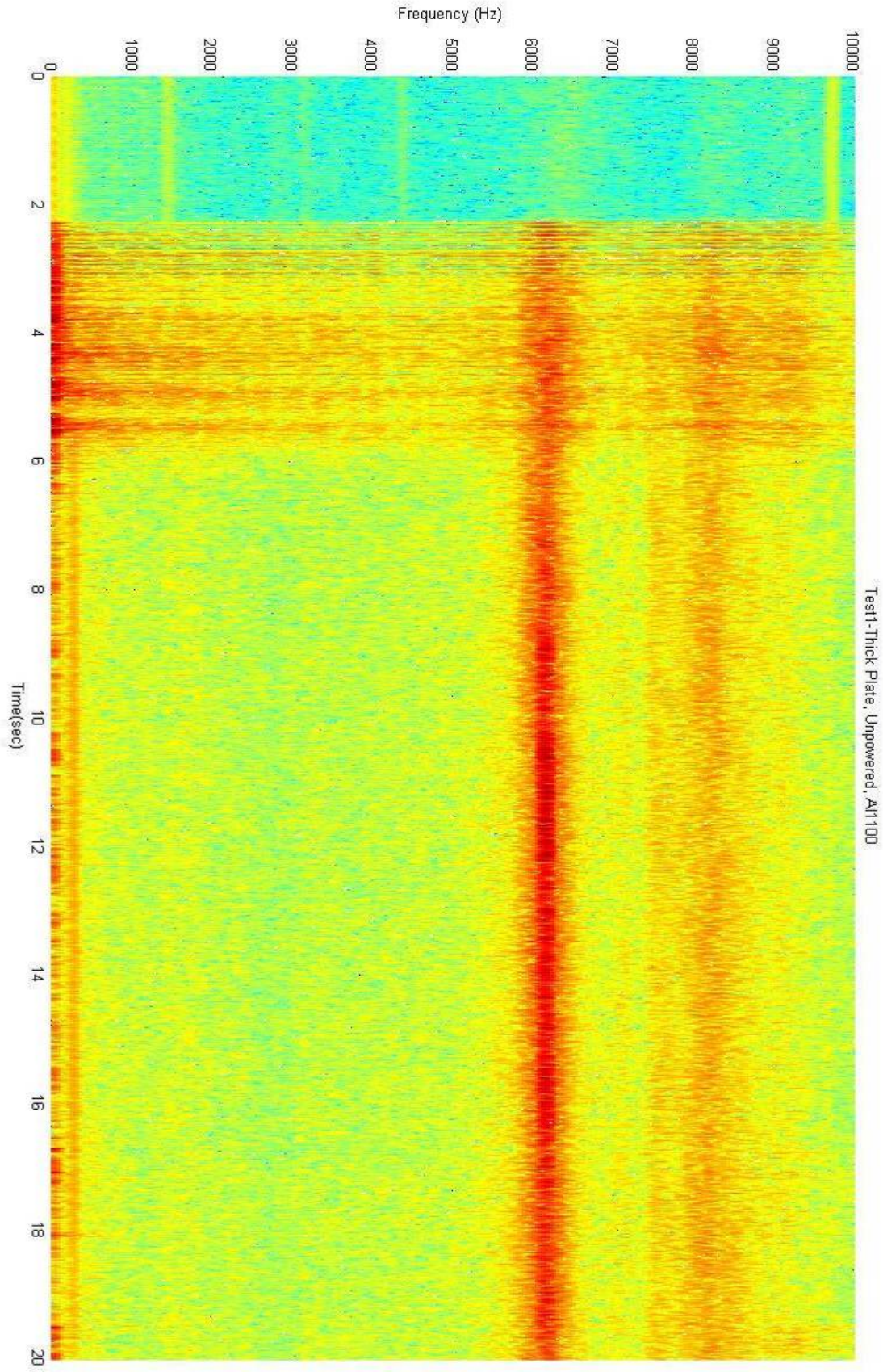

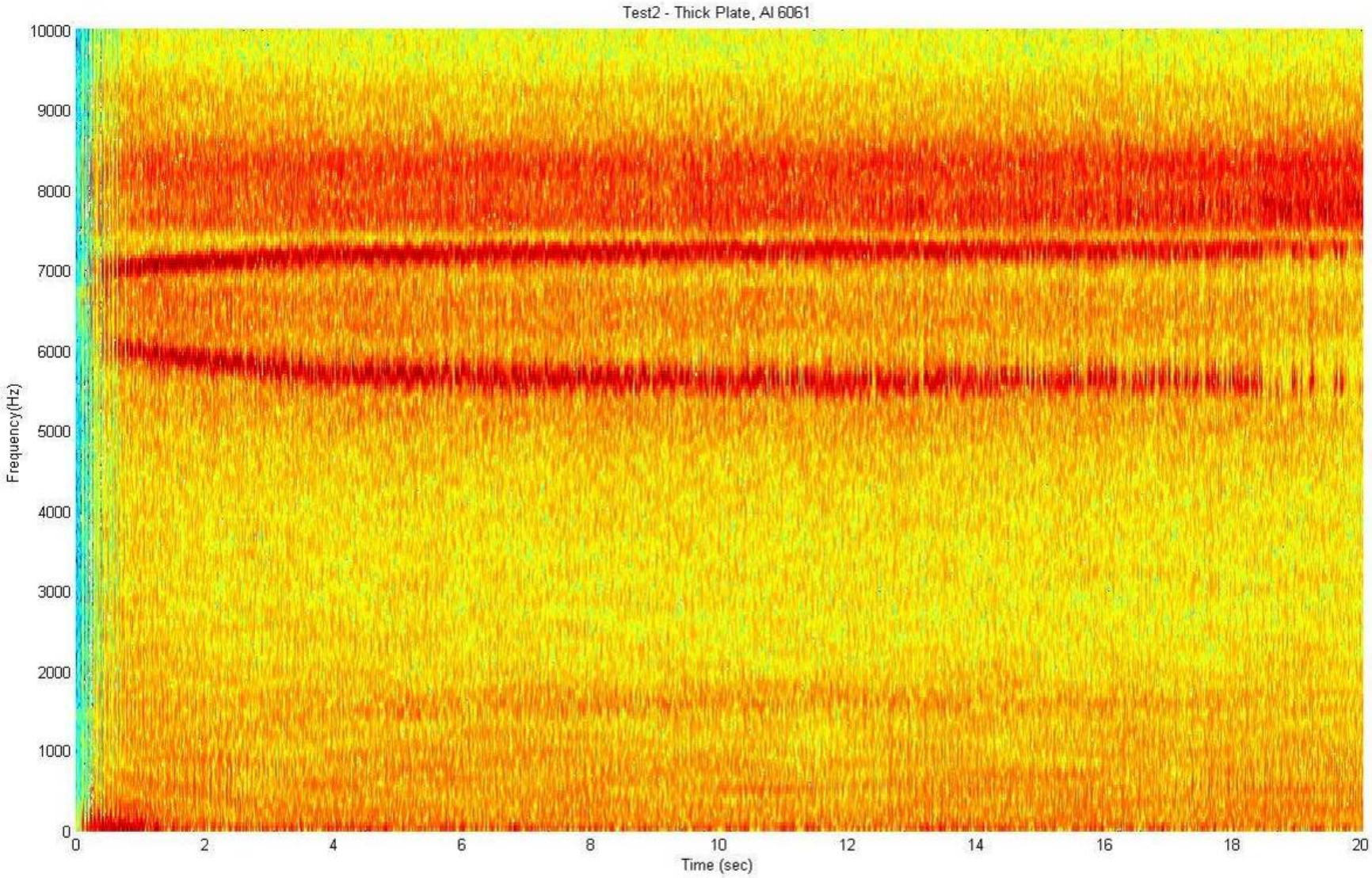
Test2 - Thick Plate, Al 6061
Frequency(Hz)
10000
9000
8000
7000
6000
5000
4000
3000
2000
1000
0
0
2
4
6
8
10
12
14
16
18
20
Time (sec)

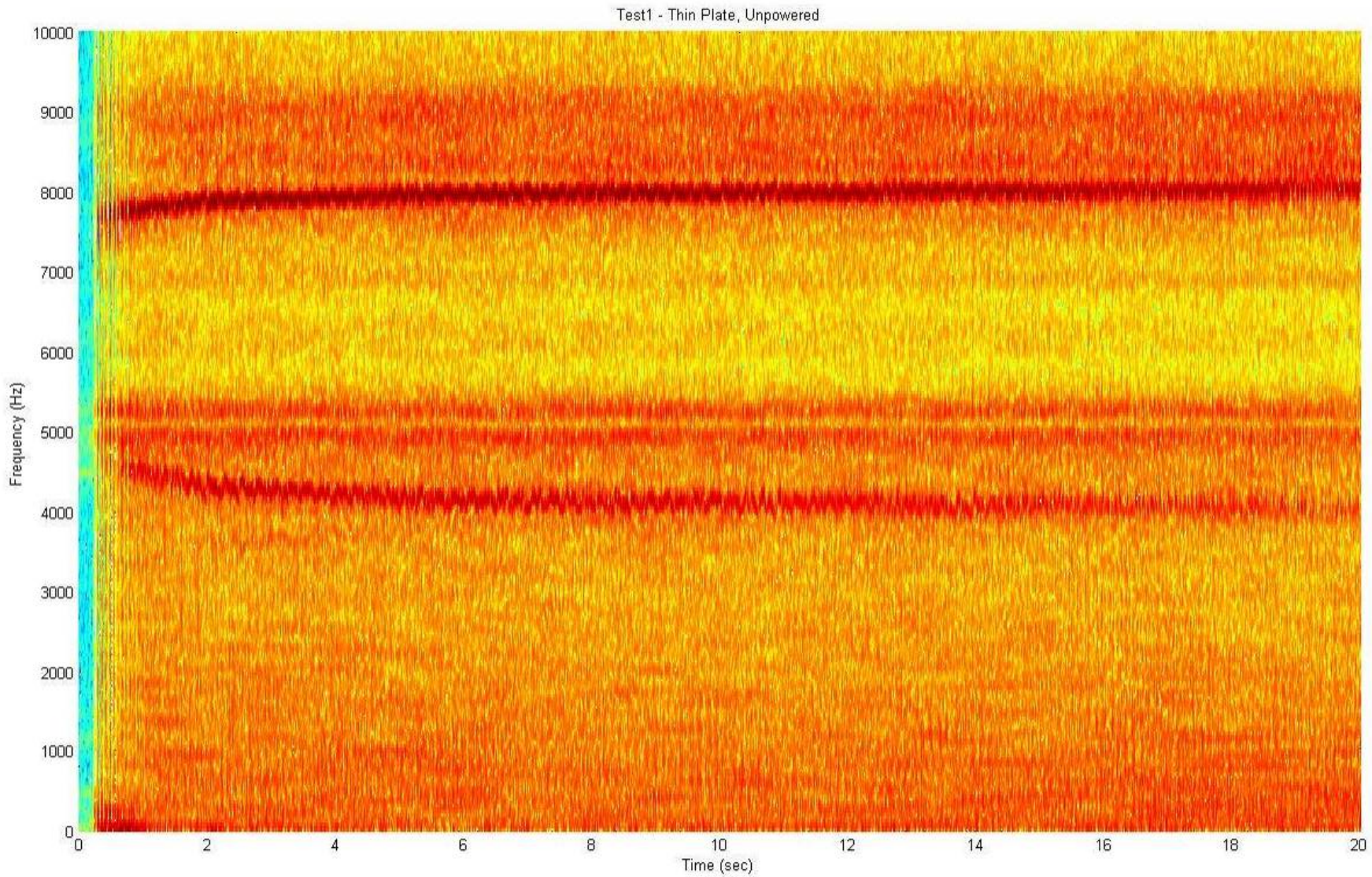
Test1 - Thin Plate, Unpowered
Frequency (Hz)
10000
9000
8000
7000
6000
5000
4000
3000
2000
1000
0
0
2
4
6
8
10
12
14
16
18
20
Time (sec)

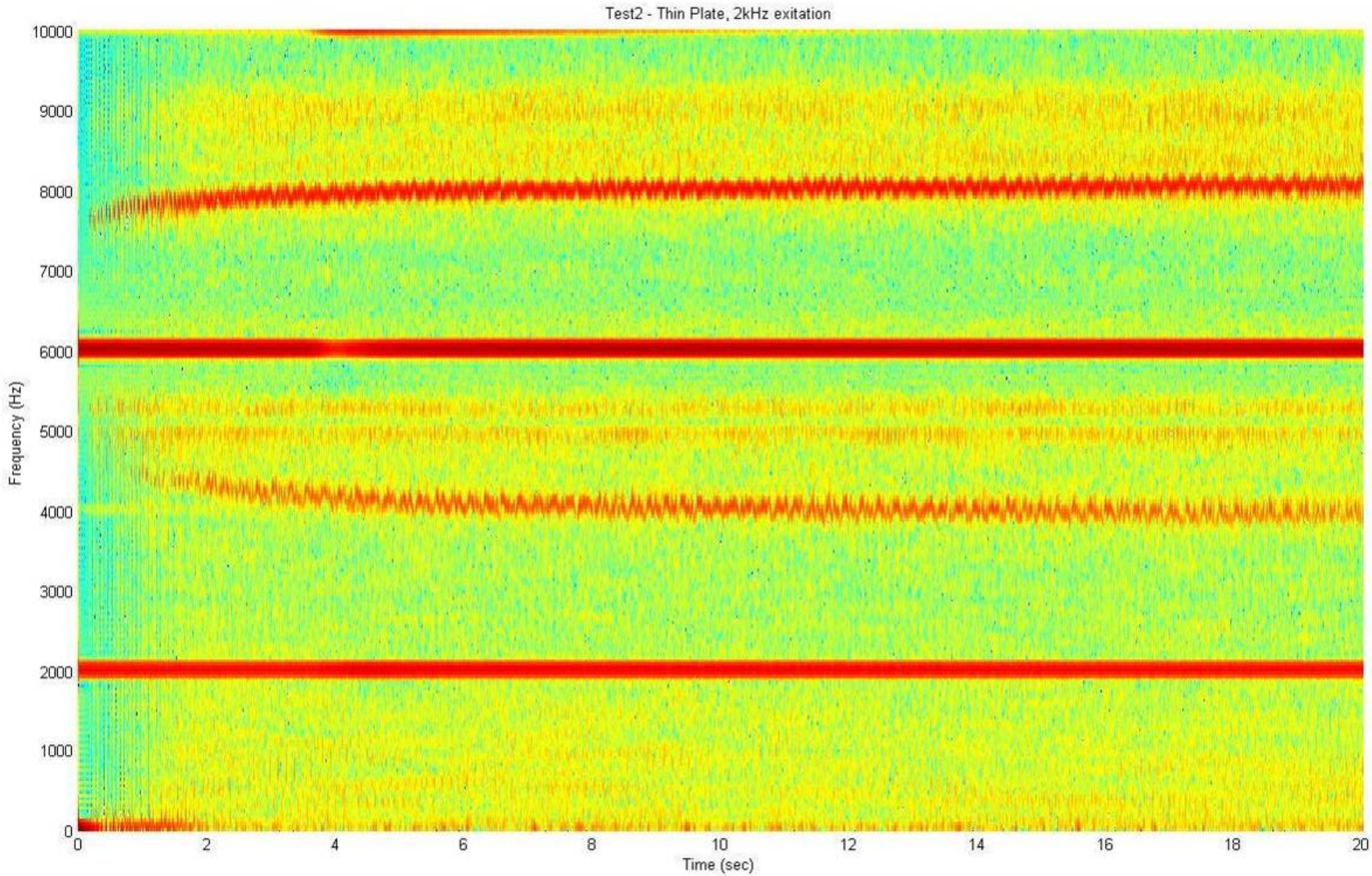
Test2 - Thin Plate, 2kHz exitation
Frequency (Hz)
10000
9000
8000
7000
6000
5000
4000
3000
2000
1000
0
0
2
4
6
8
10
12
14
16
18
20
Time (sec)

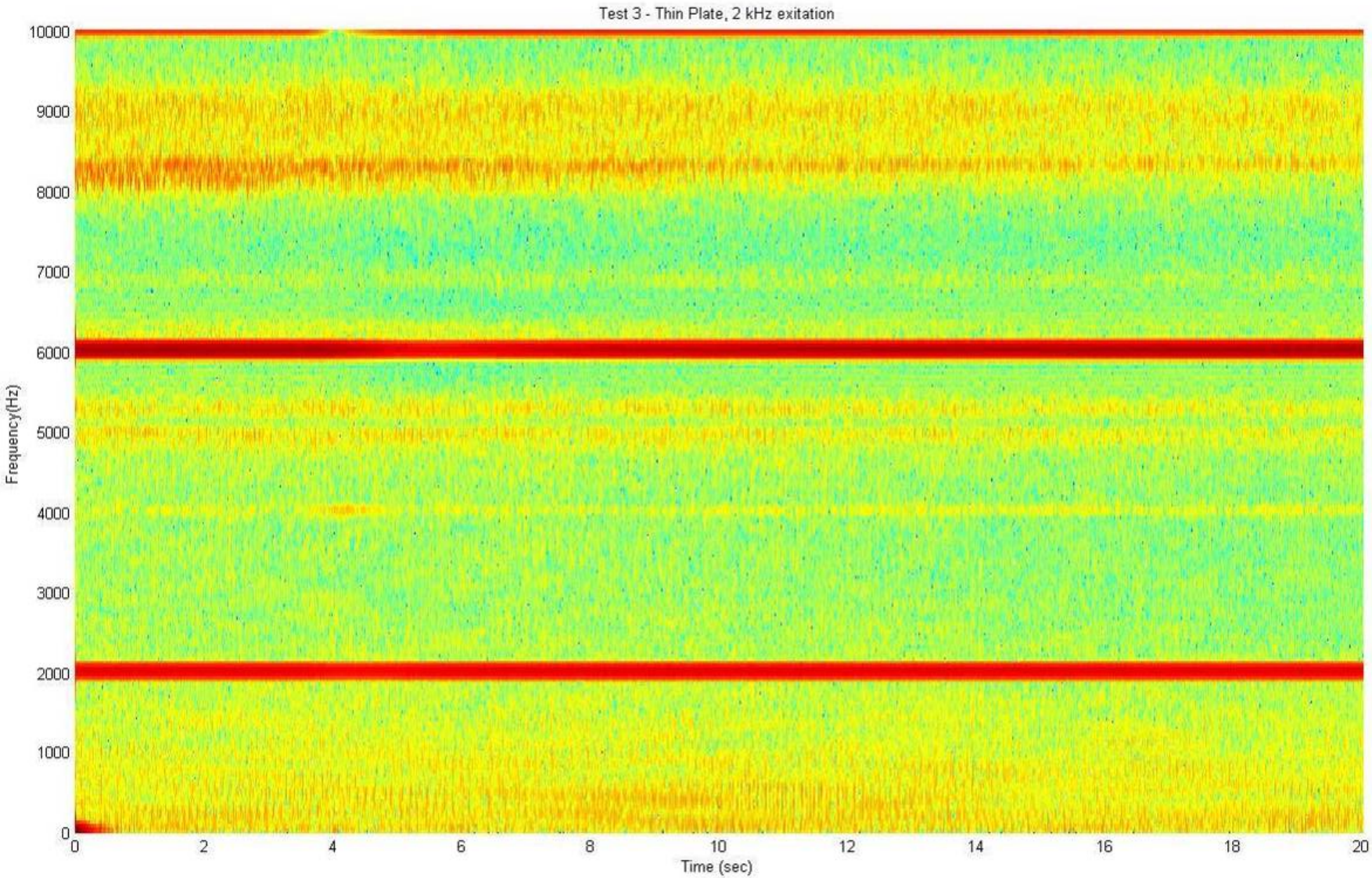
Test 3 - Thin Plate, 2 kHz exitation
Frequency(Hz)
10000
9000
8000
7000
6000
5000
4000
3000
2000
1000
0
0
2
4
6
8
10
12
14
16
18
20
Time (sec)

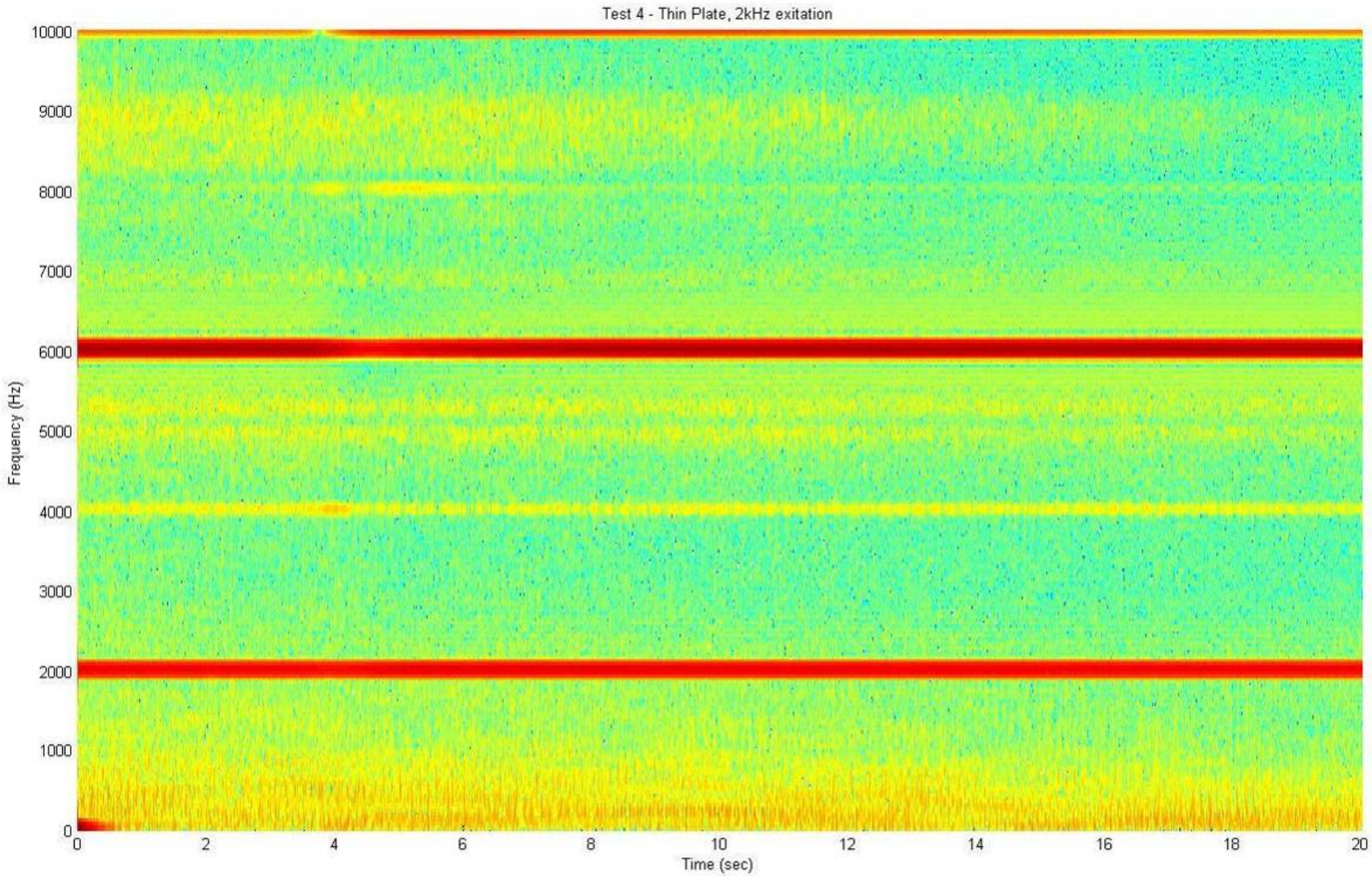
Test 4 - Thin Plate, 2kHz exitation
Frequency (Hz)
10000
9000
8000
7000
6000
5000
4000
3000
2000
1000
0
0
2
4
6
8
10
12
14
16
18
20
Time (sec)

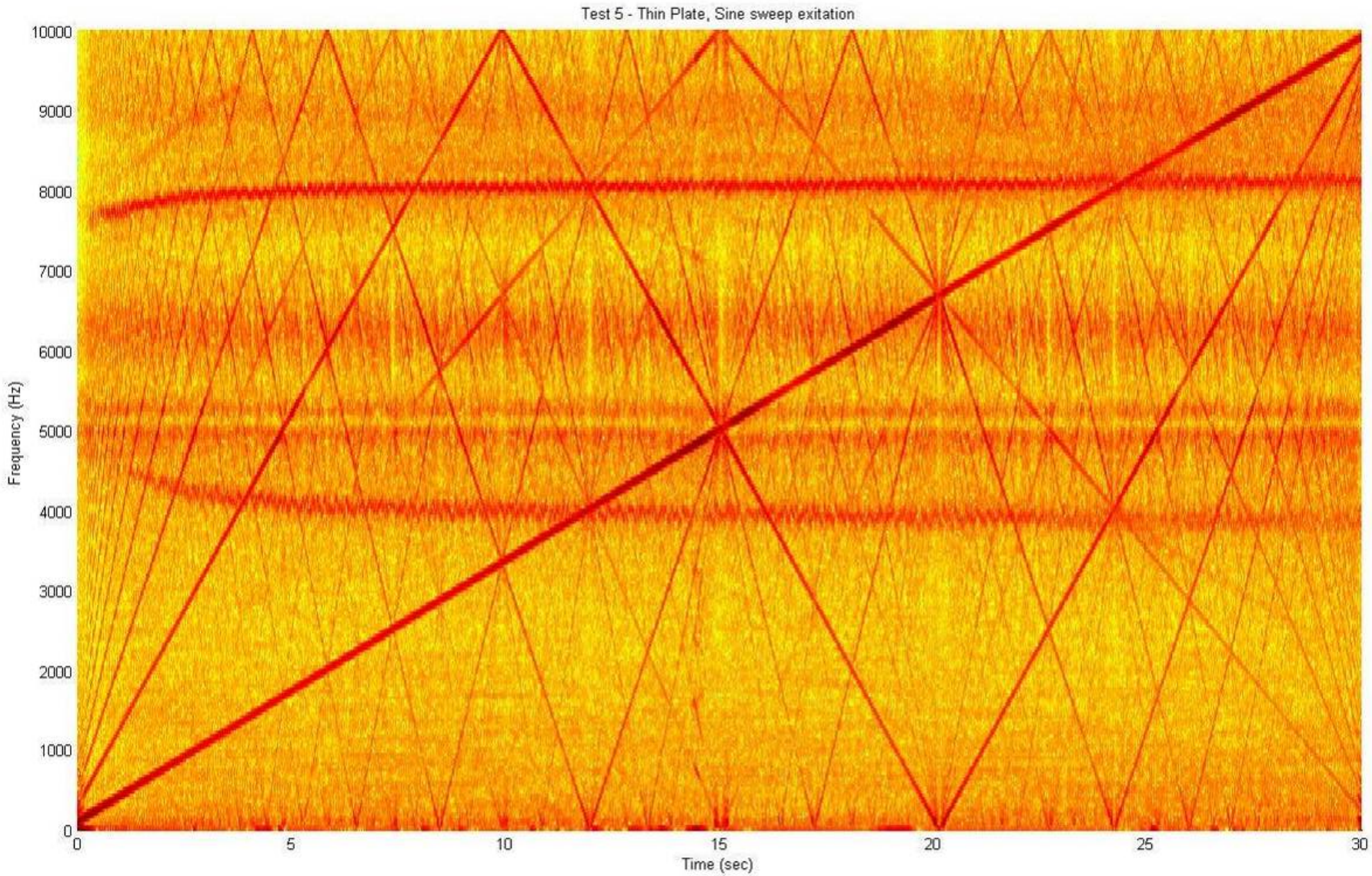
Test 5 - Thin Plate, Sine sweep exitation
Frequency (Hz)
10000
9000
8000
7000
6000
5000
4000
3000
2000
1000
0
0
5
10
15
20
25
30
Time (sec)

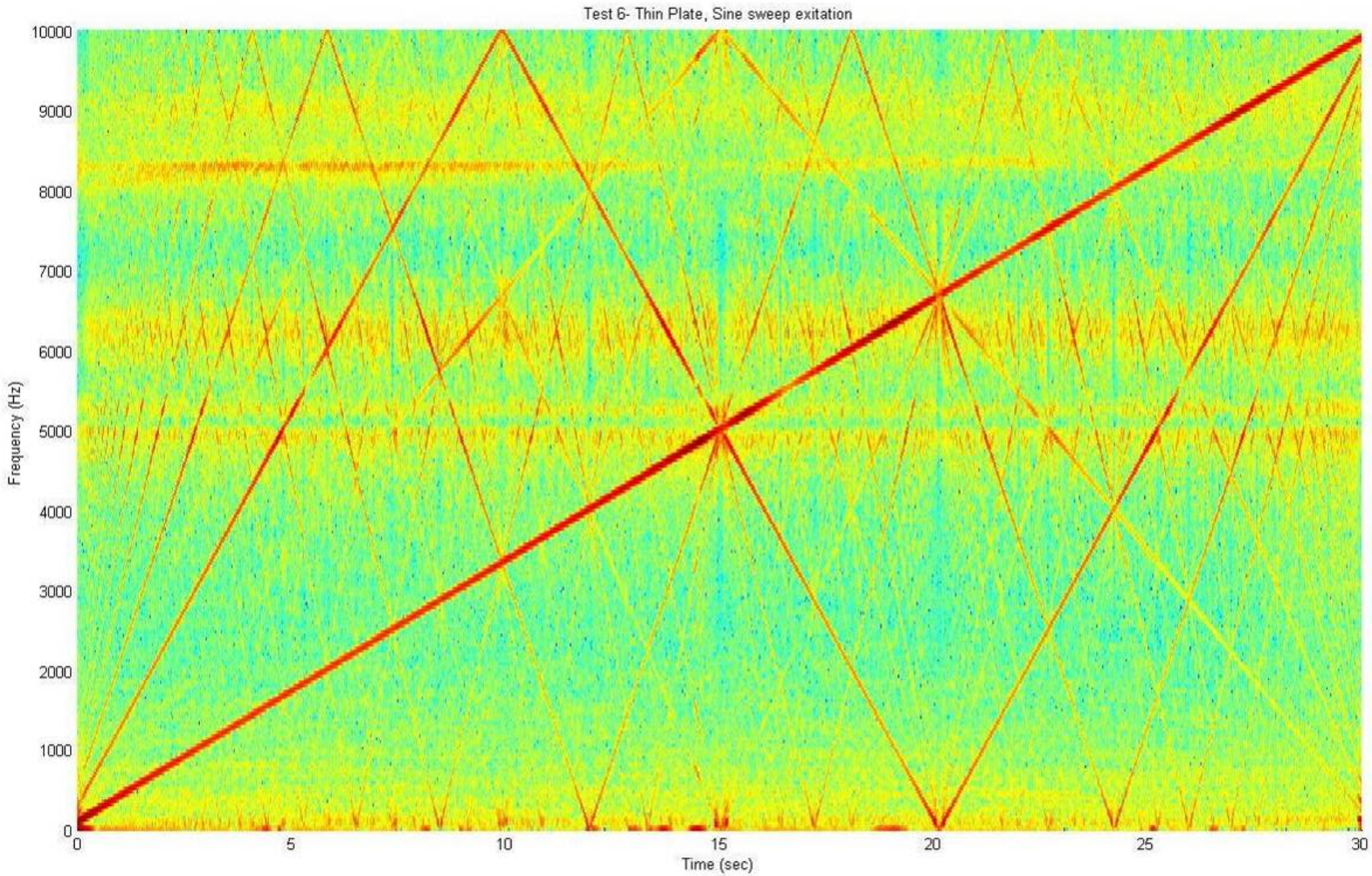
Test 6- Thin Plate, Sine sweep exitation
Frequency (Hz)
10000
9000
8000
7000
6000
5000
4000
3000
2000
1000
0
0
5
10
15
20
25
30
Time (sec)

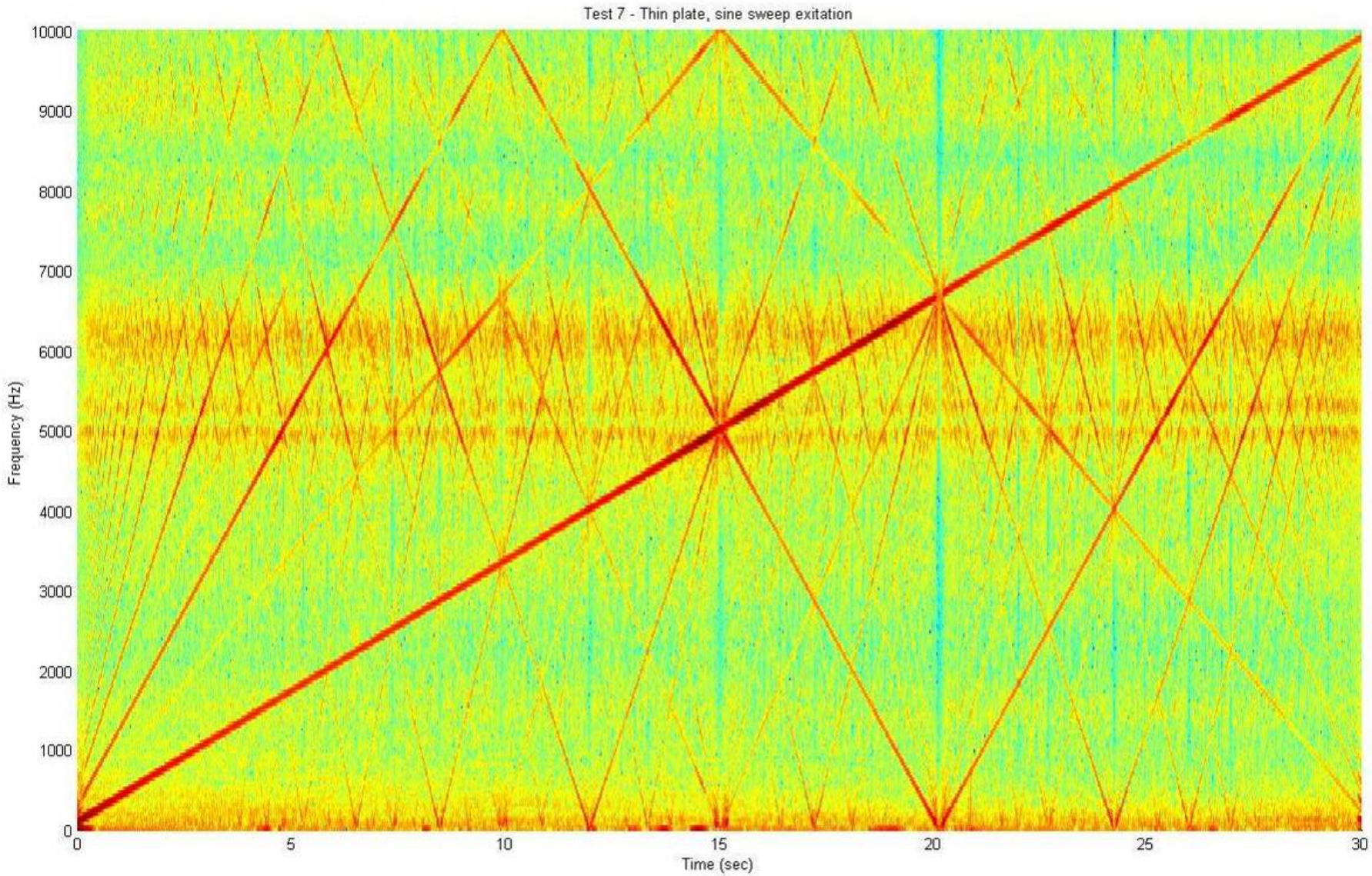
Test 7 - Thin plate, sine sweep exitation
Frequency (Hz)
10000
9000
8000
7000
6000
5000
4000
3000
2000
1000
0
0
5
10
15
20
25
30
Time (sec)

Appendix D. Surface Profilometry

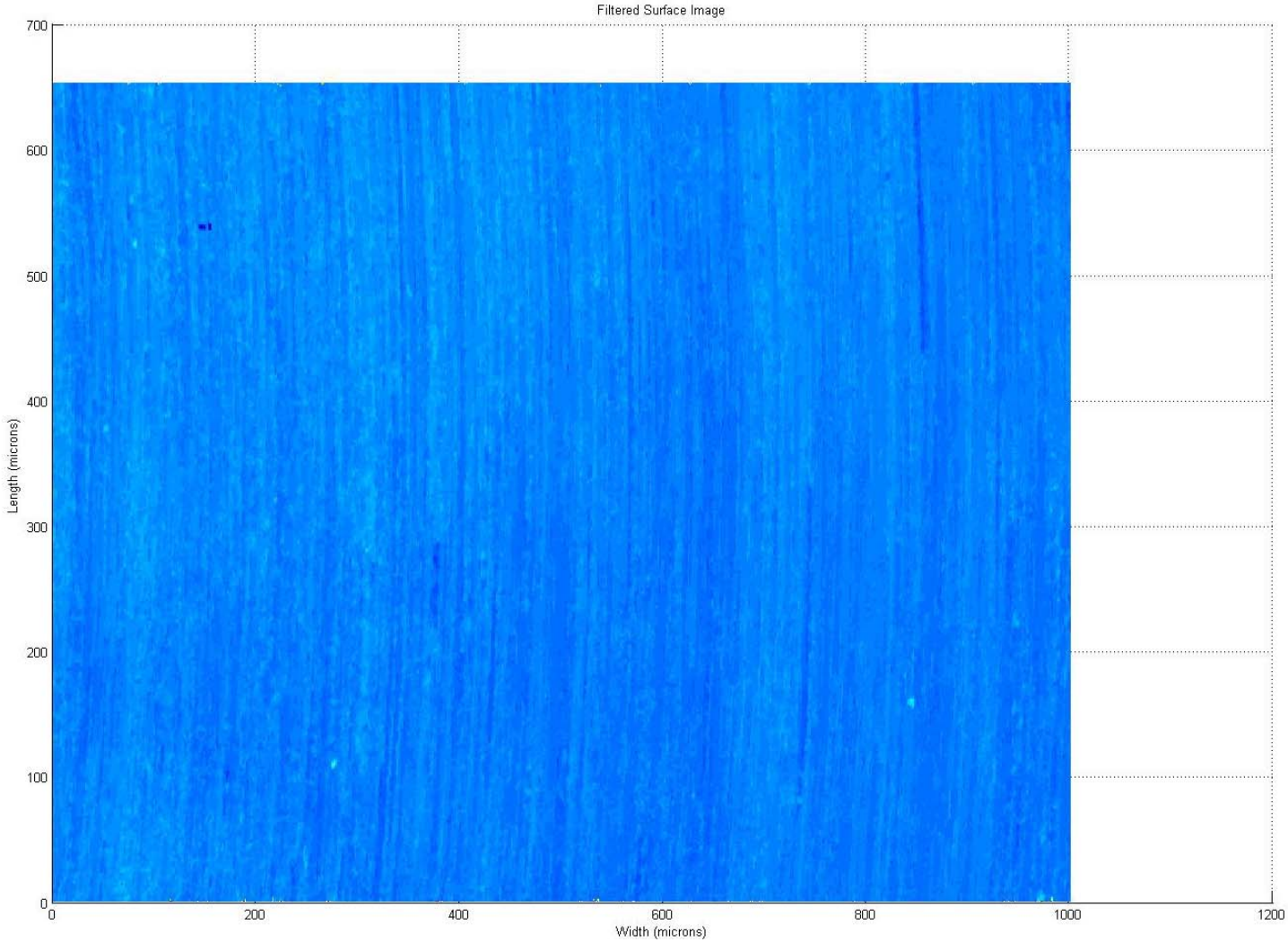

Test 1. Thick Diaphragm, Unpowered

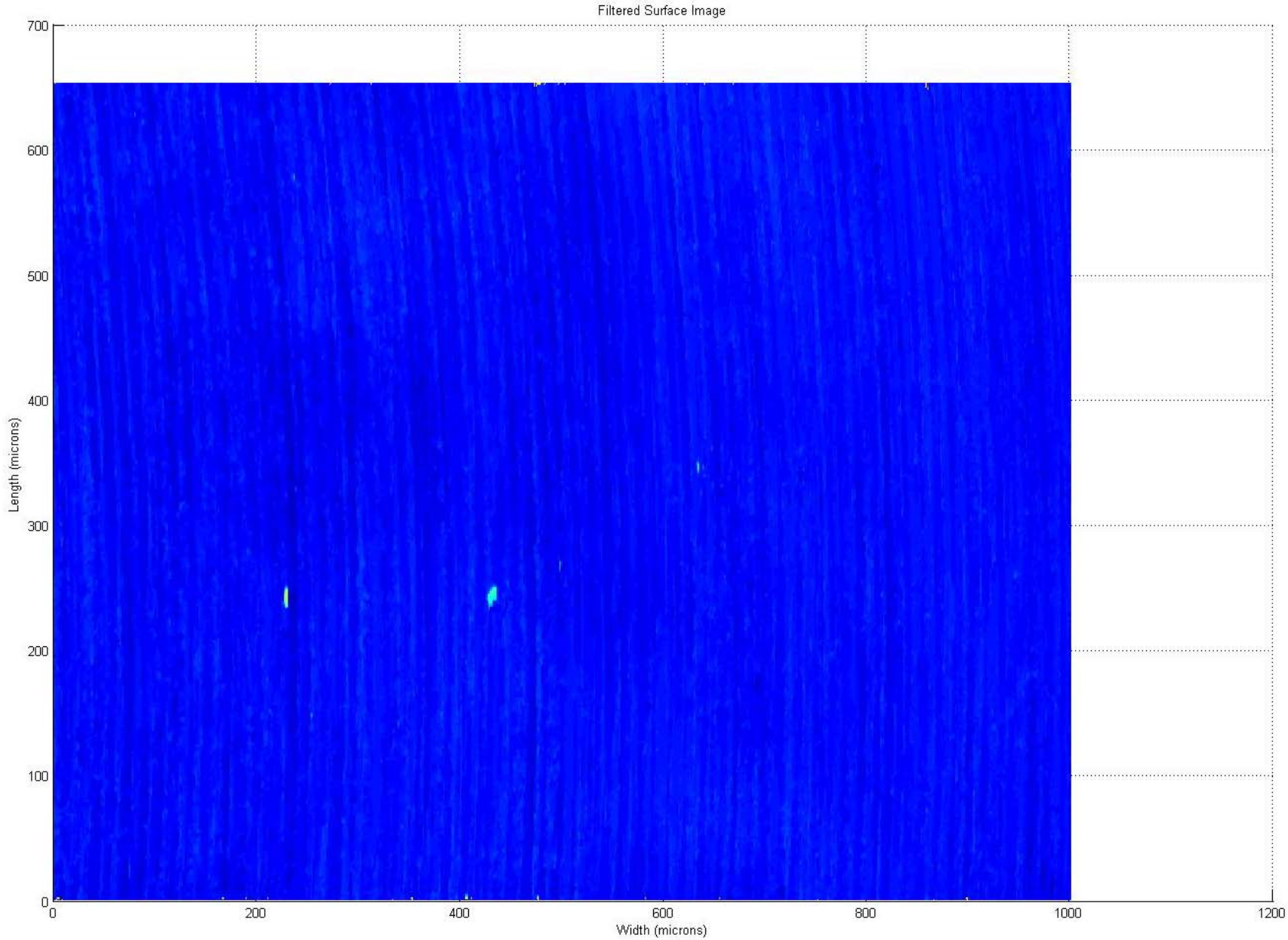

Test 2. Thin Diaphragm, Unpowered

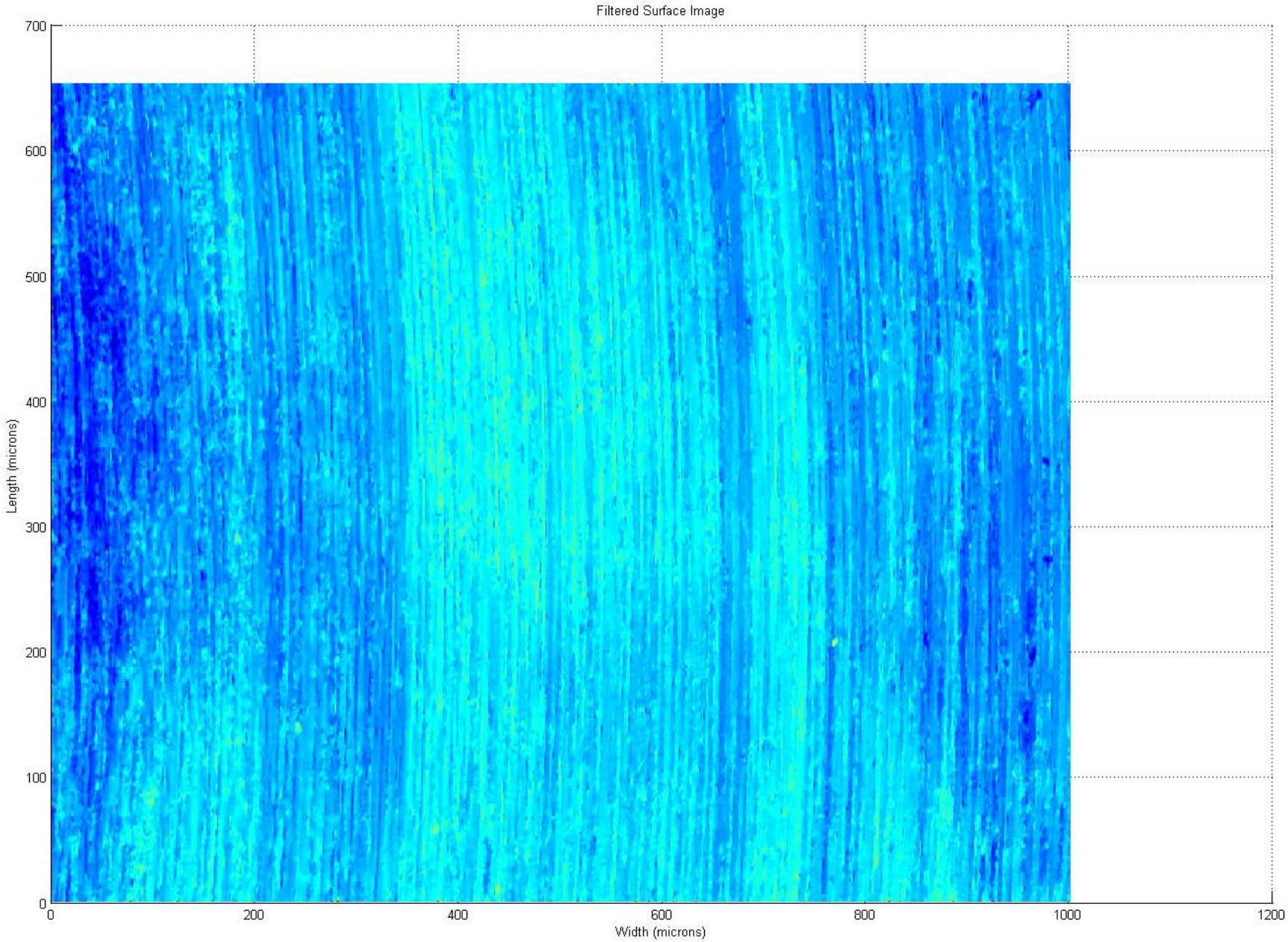

Test 3. Thin Diaphragm, 2 kHz exitation

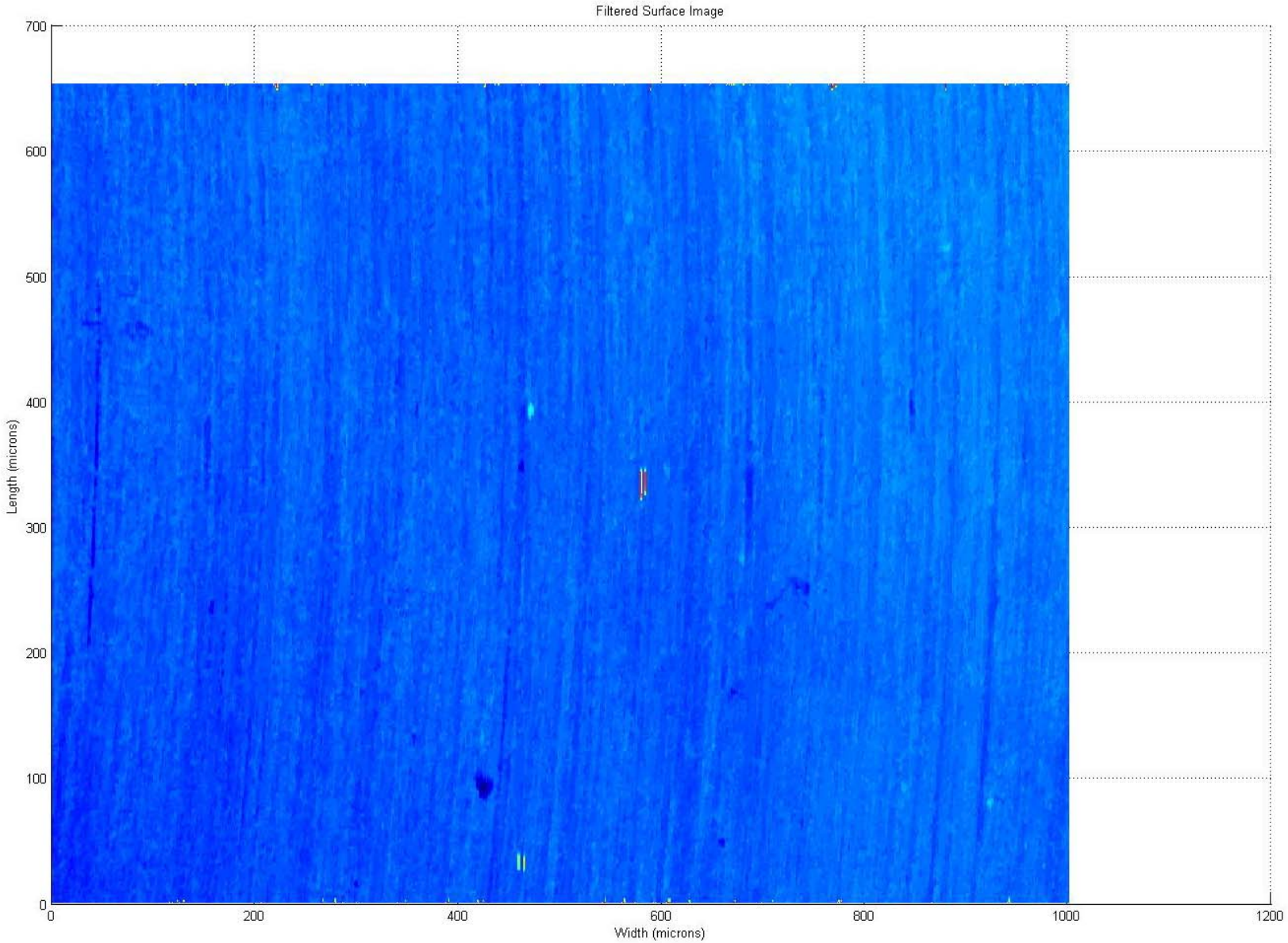

Test 4. Thin Diaphragm, 100 Hz – 10 kHz sine sweep exitation

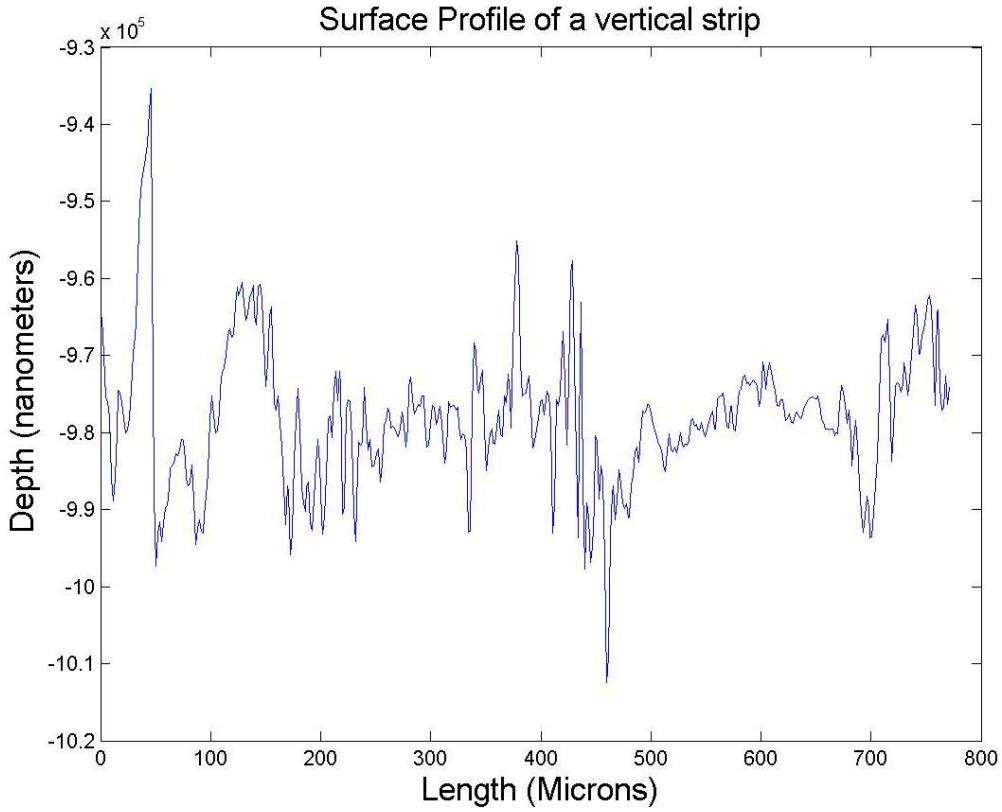

Test 1. Thick Diaphragm, Unpowered

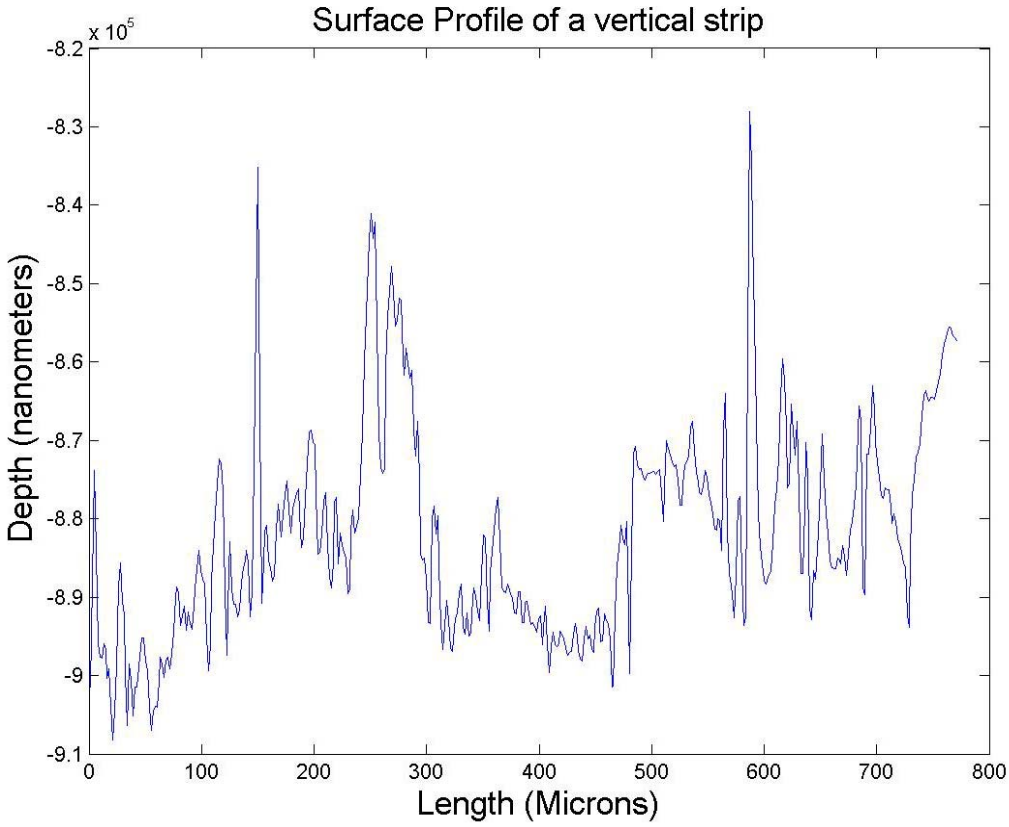

Test 2. Thin Diaphragm, Unpowered

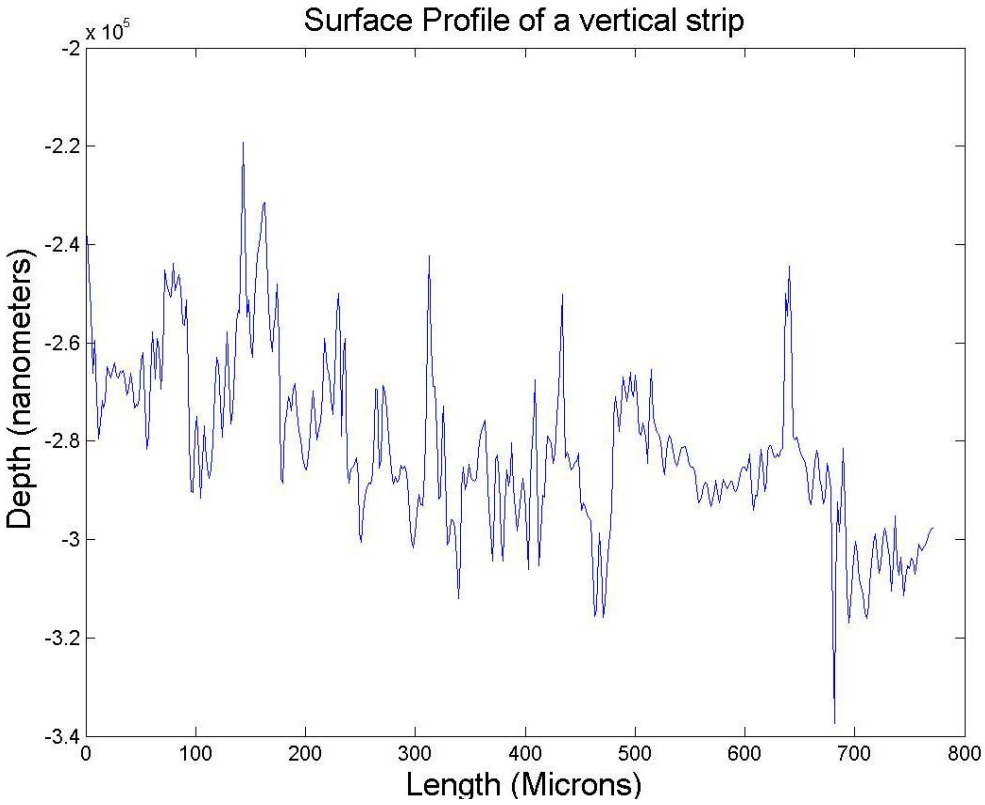

Test 3. Thin Diaphragm, 2 kHz exitation

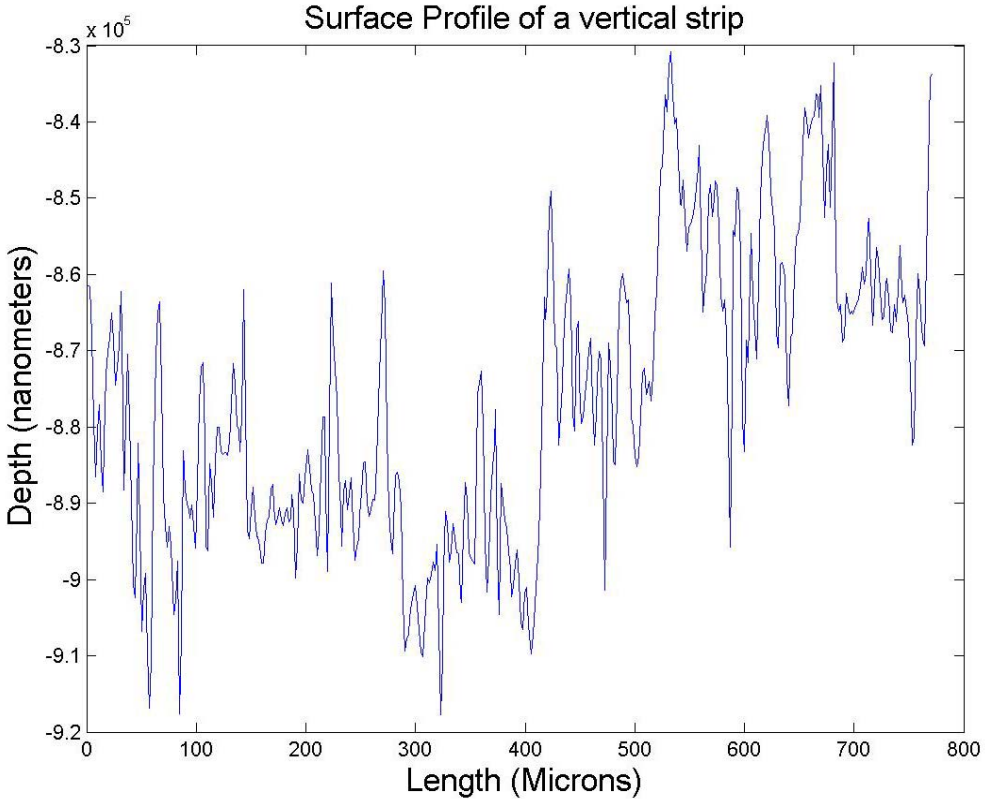

Test 4. Thin Diaphragm, 100 Hz – 10 kHz sine sweep exitation

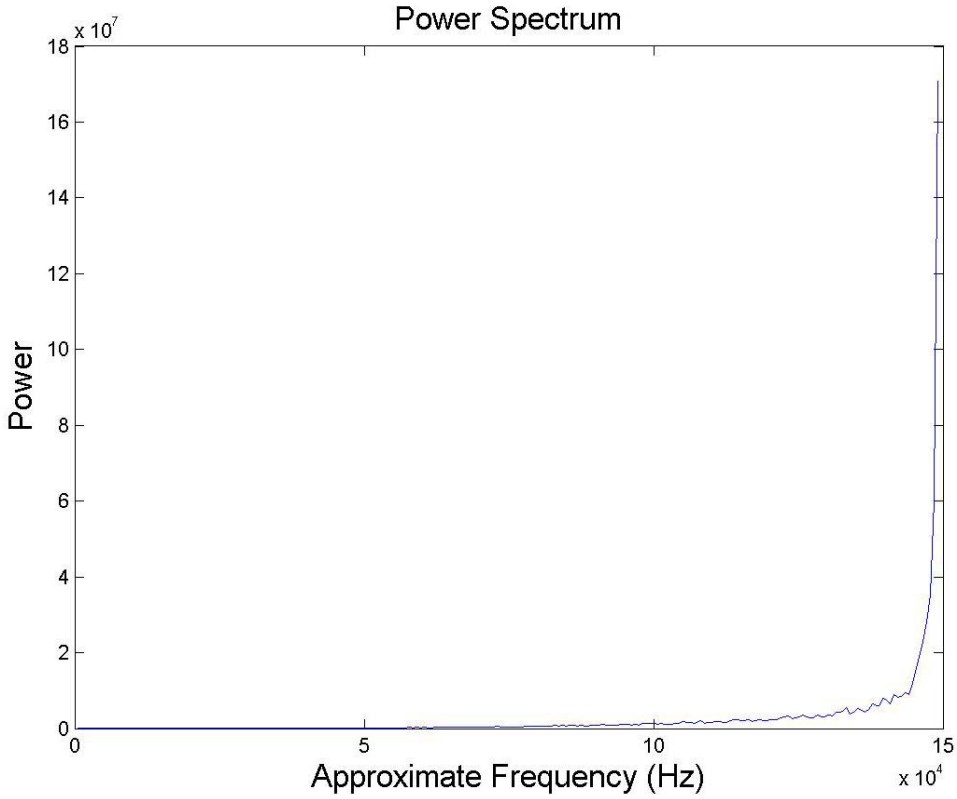

Test 1. Thick Diaphragm, Unpowered

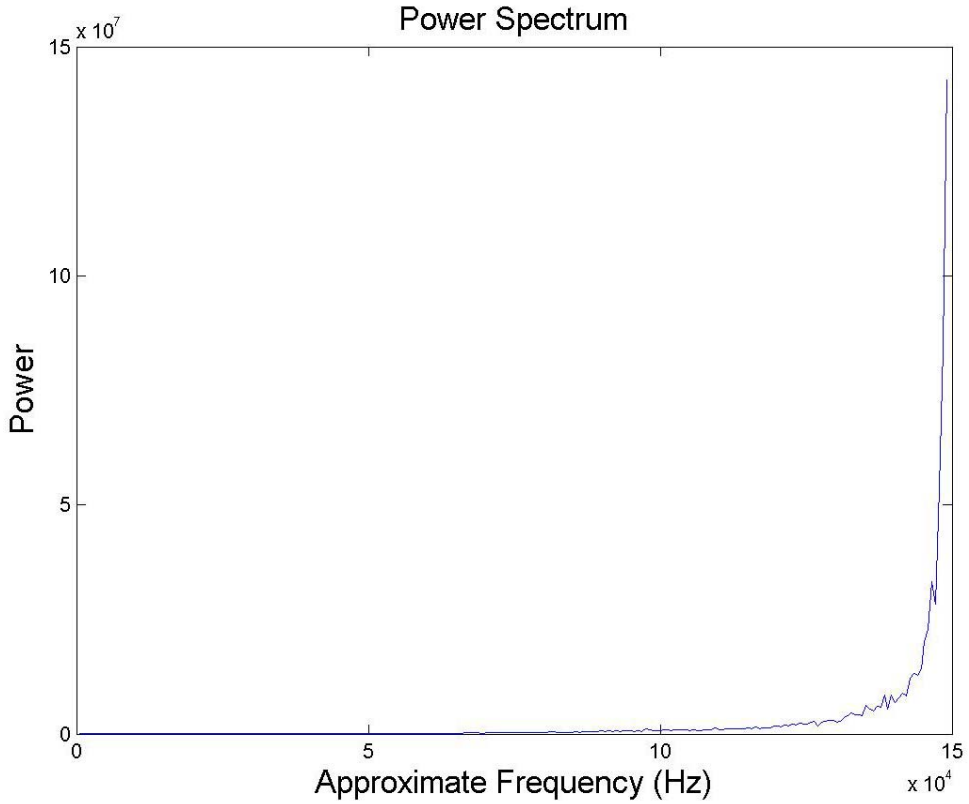

Test 2. Thin Diaphragm, Unpowered

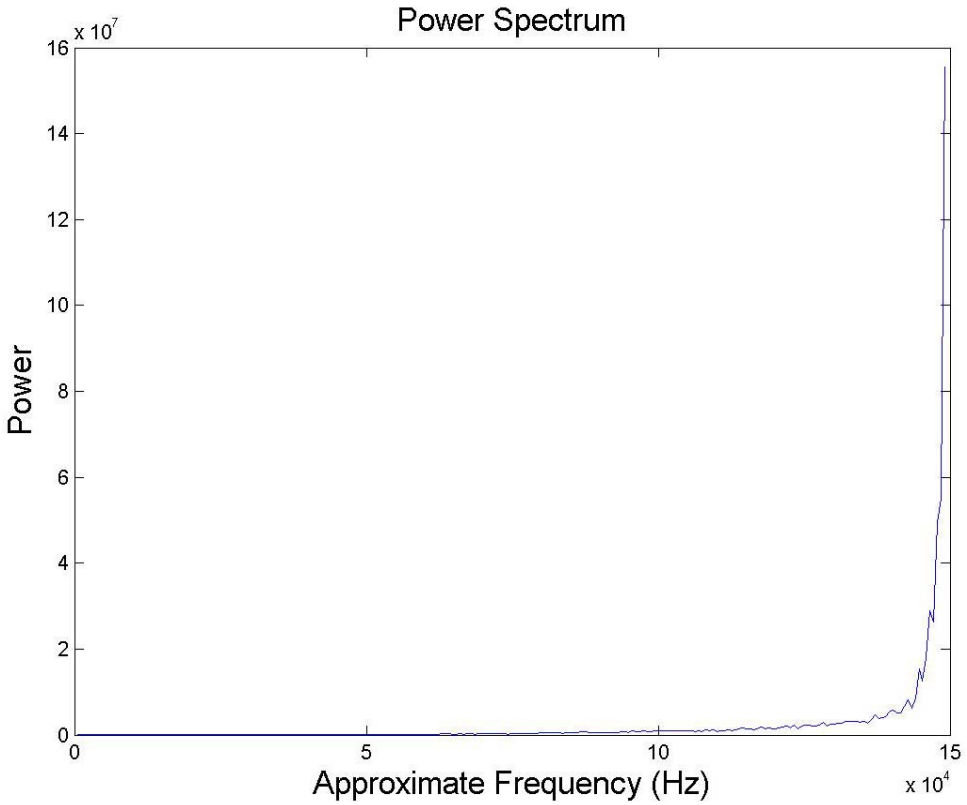

Test 3. Thin Diaphragm, 2 kHz exitation

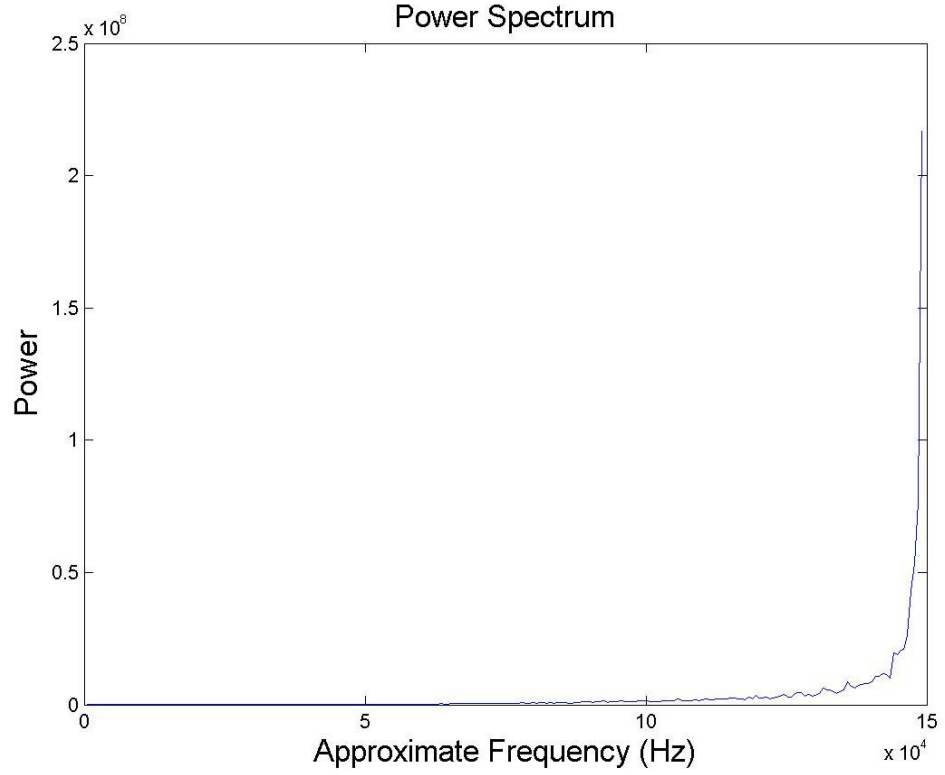

Test 4. Thin Diaphragm, 100 Hz – 10 kHz sine sweep exitation